

High Resolution Radio Astronomy Using Very Long Baseline Interferometry

Enno Middelberg and Uwe Bach*

June 10, 2022

Abstract

Very Long Baseline Interferometry, or VLBI, is the observing technique yielding the highest-resolution images today. Whilst a traditionally large fraction of VLBI observations is concentrating on Active Galactic Nuclei, the number of observations concerned with other astronomical objects such as stars and masers, and with astrometric applications, is significant. In the last decade, much progress has been made in all of these fields. We give a brief introduction into the technique of radio interferometry, focussing on the particularities of VLBI observations, and review recent results which would not have been possible without VLBI observations.

*middelberg@astro.rub.de, ubach@mpifr-bonn.mpg.de

1 Introduction

Very Long Baseline Interferometry, or VLBI, is the technique by which radio telescopes separated by up to thousands of kilometres are used at the same time for astronomical or geodetic observations. The signals are received and amplified at the participating antennas, are digitized and sent to a correlator, either by storing them on tape or disk for later shipment, or, more recently, by sending them over network links. The correlator cross-correlates and Fourier transforms the signals from each pair of antennas, and the result of this process can be used to determine the brightness distribution of the sky at radio frequencies. The angular resolution and positional accuracies achieved in these observations are as high as a fraction of a milli-arcsecond.

The radio regime was the first waveband accessible to astronomers after they had studied the skies only at optical wavelengths for hundreds of years. In the first half of the 20th century, rapid progress in high-frequency technology facilitated access to radio wavelengths. Owing to the (then) relatively long wavelengths, radio observations even with large single telescopes had poor angular resolution of no better than 10 arcmin, but after World War II the first interferometers emerged and increased the resolution to less than 1 arcmin. Astronomers were puzzled that even at the highest resolution achieved with radio-linked interferometers (about 0.1 arcsec), some radio sources appeared point-like. This fuelled the desire to use even longer baselines.

Going from directly-linked interferometers to independent elements required recording the data in some way and processing them later, but once the technical hurdles were overcome, the angular resolution of these observations increased dramatically: from 1967 to 1969, the longest baselines used in VLBI observations increased from 845 km to 10 592 km, yielding an angular resolution of the order of 1 mas. Thirty years after the first systematic radio astronomical observations had been carried out the resolution had increased more than a million fold. For more detailed reviews on radio interferometry and VLBI we refer the reader to chapter one in Thompson et al. (2001) and Kellermann and Moran (2001).

Though many important discoveries had been made early on, VLBI observations remain indispensable in many fields of astrophysical research. They will much benefit from improvements in computer technology, in particular from faster (and cheaper) network links.

This article gives a brief overview of how radio interferometry works, of the calibration and data processing steps required to make an image, and the various flavours and niches which can be explored. It then reviews recent progress in the research of various astrophysical phenomena which has been made possible with VLBI observations.

2 The theory of interferometry and aperture synthesis

2.1 Fundamentals

2.1.1 The visibility function

“An interferometer is a device for measuring the spatial coherence function” (Clark 1999). This dry statement pretty much captures what interferometry is all about, and the rest of this chapter will try to explain what lies beneath it, how the measured spatial coherence function is turned into images and how properties of the interferometer affect the images. We will mostly abstain from equations here and give a written description instead, however, some equations are inevitable. The issues explained here have been covered in length in the literature, in particular in the first two chapters of Taylor et al. (1999) and in great detail in Thompson et al. (2001).

The basic idea of an interferometer is that the spatial intensity distribution of electromagnetic radiation produced by an astronomical object at a particular frequency, I_ν , can be reconstructed from the spatial coherence function measured at two points with the interferometer elements, $V_\nu(\vec{r}_1, \vec{r}_2)$.

Let the (monochromatic) electromagnetic field arriving at the observer’s location \vec{r} be denoted by $E_\nu(\vec{r})$. It is the sum of all waves emitted by celestial bodies at that particular frequency. A property of this field is the correlation function at two points, $V_\nu(\vec{r}_1, \vec{r}_2) = \langle E_\nu(\vec{r}_1) E_\nu^*(\vec{r}_2) \rangle$, where the superscript $*$ denotes the complex conjugate. $V_\nu(\vec{r}_1, \vec{r}_2)$ describes how similar the electromagnetic field measured at two locations is. Think of two corks thrown into a lake in windy weather. If the corks are very close together, they will move up and down almost synchronously; however as their separation increases their motions will become less and less similar, until they move completely independently when several meters apart.

Radiation from the sky is largely spatially incoherent, except over very small angles on the sky, and these assumptions (with a few more) then lead to the spatial coherence function

$$V_\nu(\vec{r}_1, \vec{r}_2) \approx \int I_\nu(\vec{s}) e^{-2\pi i \nu \vec{s}(\vec{r}_1 - \vec{r}_2)/c} d\Omega \quad (1)$$

Here \vec{s} is the unit vector pointing towards the source and $d\Omega$ is the surface element of the celestial sphere. The interesting point of this equation is that it is a function of the separation and relative orientation of two locations. An interferometer in Europe will measure the same thing as one in Australia, provided the separation and orientation of the interferometer elements are the same. The relevant parameters here are the coordinates of the antennas when projected onto a plane perpendicular to the line of sight (Figure 1). This plane has the axes u and v , hence it is called the (u, v) plane. Now let us further introduce units of wavelengths to measure positions in the (u, v) plane. One then gets

$$V_\nu(u, v) = \iint I_\nu(l, m) e^{-2\pi i(ul+vm)} dl dm \quad (2)$$

This equation is a Fourier transform between the spatial coherence function and the (modified) intensity distribution in the sky, I_ν , and can be inverted to obtain I_ν . The coordinates u and v are the components of a vector pointing from the origin of the (u, v) plane to a point in the plane, and describe the projected separation and orientation of the elements, measured in wavelengths. The coordinates l and m are direction cosines towards the astronomical source (or a part thereof). In radio astronomy, V_ν is called the visibility function, but a factor, A_ν , is commonly included to describe the sensitivity of the interferometer elements as a function of angle on the sky (the antenna response¹).

$$V_\nu(u, v) = \iint A_\nu(l, m) I_\nu(l, m) e^{-2\pi i(ul+vm)} dl dm \quad (3)$$

The visibility function is the quantity all interferometers measure and which is the input to all further processing by the observer.

2.1.2 The (u, v) plane

We introduced a coordinate system such that the line connecting the interferometer elements, the baseline, is perpendicular to the direction towards the source, and this plane is called the (u, v) plane for obvious reasons. However, the baseline in the (u, v) plane is only a projection of the vector connecting the physical elements. In general, the visibility function will not be the same at different locations in the (u, v) plane, an effect arising from structure in the astronomical source. It is therefore desirable to measure it at as many points in the (u, v) plane as possible. Fortunately, the rotation of the earth continuously changes the relative orientation of the interferometer elements with respect to the source, so that the point given by (u, v) slowly rotates through the plane, and so an interferometer which is fixed on the ground samples various aspects of the astronomical source as the observation progresses. Almost all contemporary radio interferometers work in this way, and the technique is then called aperture synthesis. Furthermore, one can change the observing frequency to move (radially) to a different point in the (u, v) plane. This is illustrated in Figure 2. Note that the visibility measured at $(-u, -v)$ is the complex conjugate of that measured at (u, v) , and therefore does not add information. Hence sometimes in plots of (u, v) coverage such as Figure 2, one also plots those points mirrored across the origin. A consequence of this relation is that after 12 h the aperture synthesis with a given array and frequency is complete.

¹The fields of view in VLBI observations are typically so small that the dependence of (l, m) can be safely ignored. A_ν can then be set to unity and disappears.

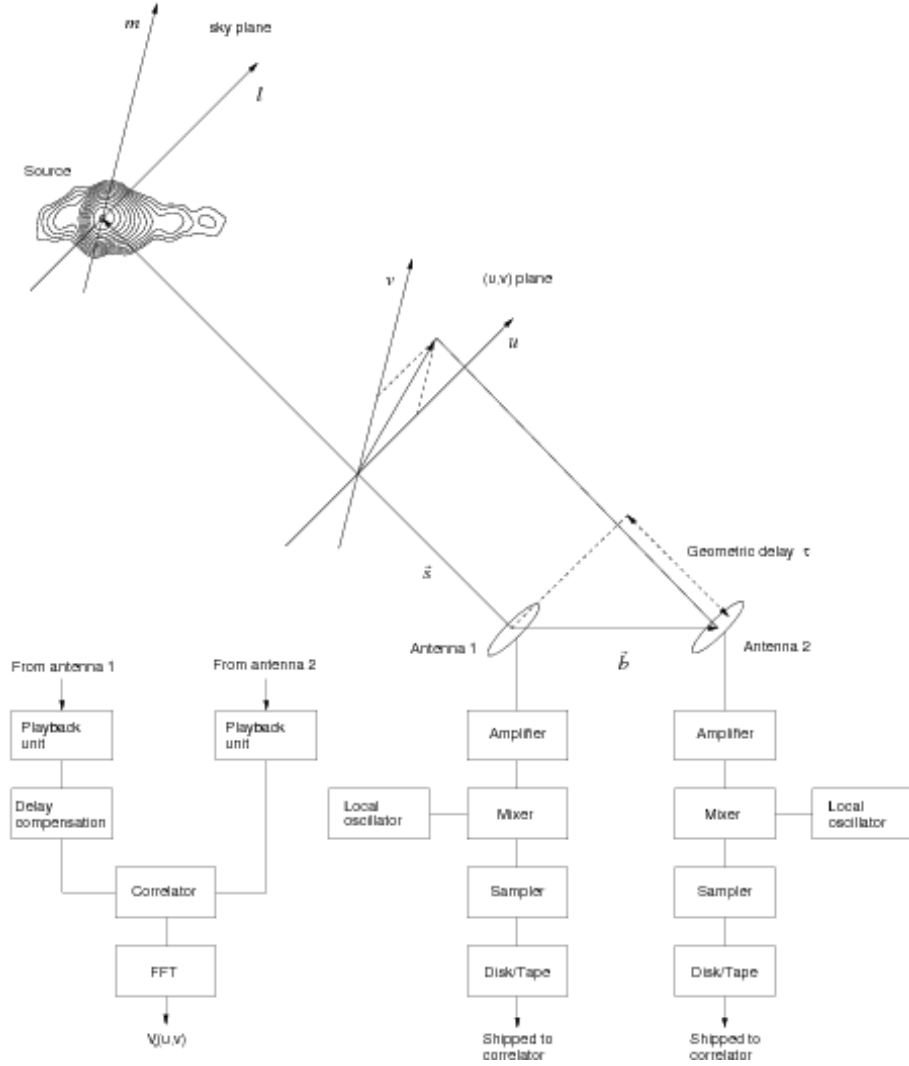


Figure 1: Sketch of how a visibility measurement is obtained from a VLBI baseline. The source is observed in direction of the line-of-sight vector, \vec{s} , and the sky coordinates are the direction cosines l and m . The projection of the station coordinates onto the (u, v) plane, which is perpendicular to \vec{s} , yields the (u, v) coordinates of the antennas, measured in units of the observing wavelength. The emission from the source is delayed at one antenna by an amount $\tau = \vec{s} \times \vec{b}/c$. At each station, the signals are intercepted with antennas, amplified, and then mixed down to a low frequency where they are further amplified and sampled. The essential difference between a connected-element interferometer and a VLBI array is that each station has an independent local oscillator, which provides the frequency normal for the conversion from the observed frequency to the recorded frequency. The sampled signals are written to disk or tape and shipped to the correlator. At the correlator, the signals are played back, the geometric delay τ is compensated for, and the signals are correlated and Fourier transformed (in the case of an XF correlator).

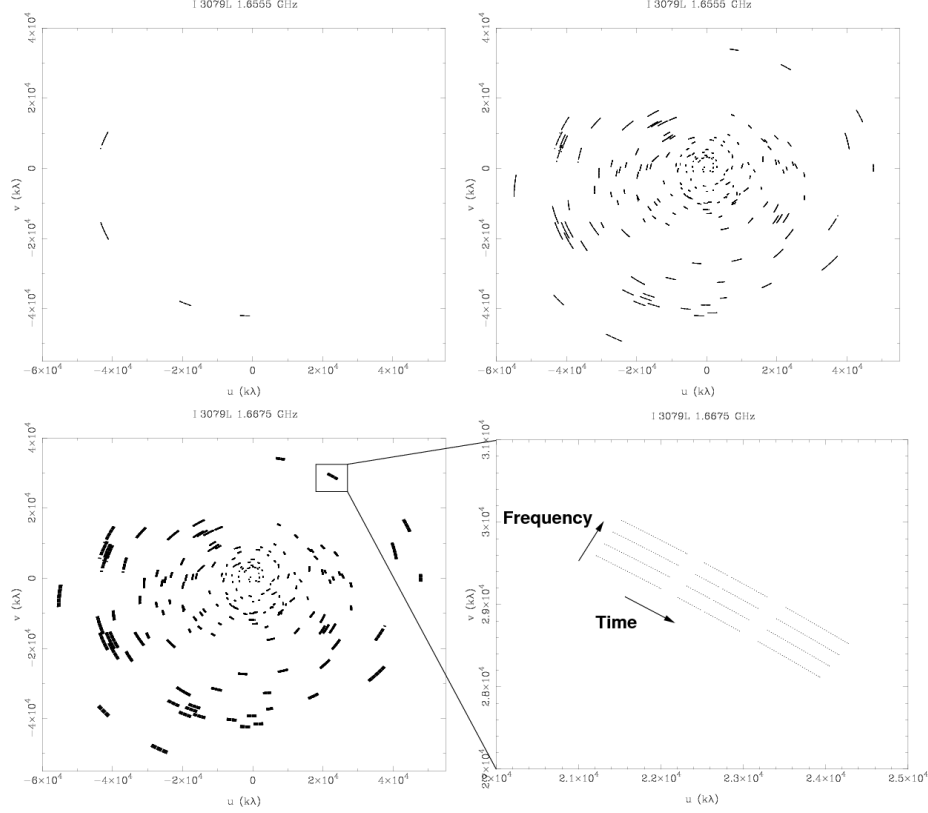


Figure 2: Points in the (u, v) plane sampled during a typical VLBI observation at a frequency of 1.7 GHz ($\lambda=0.18$ m). The axis units are kilolambda, and the maximum projected baseline length corresponds to $60000 k\lambda=10800$ km. The source was observed four times for 25 min each, over a time range of 7.5 h. For each visibility only one point has been plotted, i.e., the locations of the complex conjugate visibilities are not shown. *Top left:* The (u, v) track of a single baseline. It describes part of an ellipse the centre of which does not generally coincide with the origin (this is only the case for an east-west interferometer). *Top right:* The (u, v) track of all interferometer pairs of all participating antennas. *Bottom left:* The same as the top right panel, but the (u, v) points of all four frequency bands used in the observation have been plotted, which broadened the tracks. *Bottom right:* This plot displays a magnified portion of the previous diagram. It shows that at any one time the four frequency bands sample different (u, v) points which lie on concentric ellipses. As the Earth rotates, the (u, v) points progress tangentially.

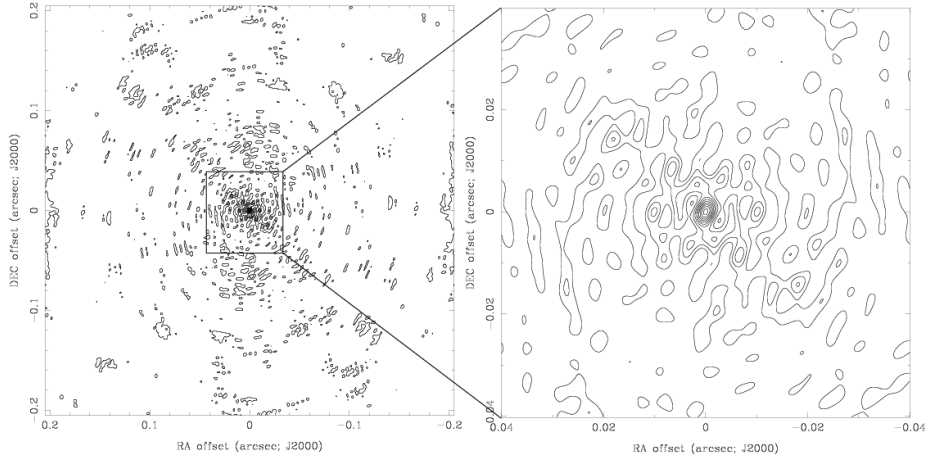


Figure 3: The PSF $B(l, m)$ of the (u, v) coverage shown in the bottom left panel of Figure 2. Contours are drawn at 5 %, 15 %, 25 %, ... of the peak response in the image centre. Patches where the response is higher than 5 % are scattered all over the image, sometimes reaching 15 %. In the central region, the response outside the central peak reaches more than 25 %. Without further processing, the achievable dynamic range with this sort of PSF is of the order of a few tens.

2.1.3 Image reconstruction

After a typical VLBI observation of one source, the (u, v) coverage will not look too different from the one shown in Figure 2. These are all the data needed to form an image by inverting Equation 3. However, the (u, v) plane has been sampled only at relatively few points, and the purely Fourier-transformed image (the “dirty image”) will look poor. This is because the true brightness distribution has been convolved with the instrument’s point-spread function (PSF). In the case of aperture synthesis, the PSF $B(l, m)$ is the Fourier transform of the (u, v) coverage:

$$B(l, m) = F(S(u, v)) \quad (4)$$

Here $S(u, v)$ is unity where measurements have been made, and zero elsewhere. Because the (u, v) coverage is mostly unsampled, $B(l, m)$ has very high artefacts (“sidelobes”).

To remove the sidelobes requires to interpolate the visibilities to the empty regions of the (u, v) plane, and the standard method in radio astronomy to do that is the “CLEAN” algorithm.

2.1.4 CLEAN

The CLEAN algorithm (Högbom 1974) is a non-linear, iterative mechanism to rid interferometry images of artefacts caused by insufficient (u, v) coverage.

Although a few varieties exist the basic structure of all CLEAN implementations is the same:

- Find the brightest pixel $I'(l_i, m_i)$ in the dirty image.
- Translate the dirty beam $B(l, m) = F(S(u, v))$ so that the centre pixel is at the same location as $I'(l_i, m_i)$ and scale it with a factor c so that $I'(l_i, m_i) = cB(l_i + \Delta l, m_i + \Delta m)$.
- Subtract from each pixel in the dirty image the corresponding value in the dirty beam, multiplied by a previously defined loop gain value $\gamma < 1$ and keep the residual: $R(l, m) = I'(l, m) - c\gamma B(l + \Delta l, m + \Delta m)$
- Add the model component $(l_i, m_i, \gamma I'(l_i, m_i))$ as a delta component to the “clean image” and start over again.

CLEAN can be stopped when the sidelobes of the sources in the residual image are much lower than the image noise. A corollary of this is that in the case of very low signal-to-noise ratios CLEAN will essentially have no effect on the image quality, because the sidelobes are below the noise limit introduced by the receivers in the interferometer elements. The “clean image” is iteratively build up out of delta components, and the final image is formed by convolving it with the “clean beam”. The clean beam is a two-dimensional Gaussian which is commonly obtained by fitting a Gaussian to the centre of the dirty beam image. After the convolution the residual image is added.

The way in which images are formed in radio interferometry may seem difficult and laborious (and it is), but it also adds great flexibility. Because the image is constructed from typically thousands of interferometer measurements one can choose to ignore measurements from, e.g., the longest baselines to emphasize sensitivity to extended structure. Alternatively, one can choose to weight down or ignore short spacings to increase resolution. Or one can convolve the clean model with a Gaussian which is much smaller than the clean beam, to make a clean image with emphasis on fine detail (“superresolution”).

2.1.5 Generating a visibility measurement

The previous chapter has dealt with the fundamentals of interferometry and image reconstruction. In this chapter we will give a brief overview about more technical aspects of VLBI observations and the signal processing involved to generate visibility measurements.

It may have become clear by now that an interferometer array really is only a collection of two-element interferometers, and only at the imaging stage is the information gathered by the telescopes combined. In an array of N antennas, the number of pairs which can be formed is $N(N - 1)/2$, and so an array of 10 antennas can measure the visibility function at 45 locations in the (u, v) plane simultaneously. Hence, technically, obtaining visibility measurements with a global VLBI array consisting of 16 antennas is no more complex than doing it with a two-element interferometer - it is just logistically more challenging.

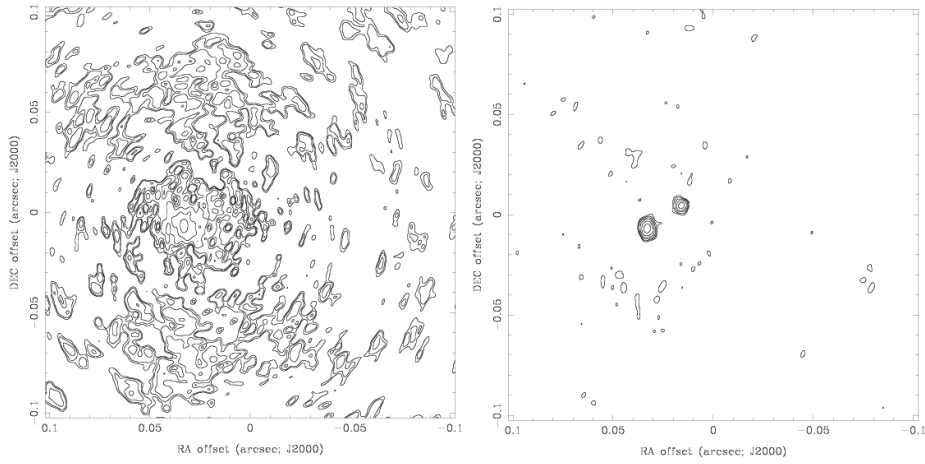


Figure 4: Illustration of the effects of the CLEAN algorithm. *Left panel:* The Fourier transform of the visibilities already used for illustration in Figures 2 and 3. The image is dominated by artefacts arising from the PSF of the interferometer array. The dynamic range of the image (the image peak divided by the rms in an empty region) is 25. *Right panel:* The “clean image”, made by convolving the model components with the clean beam, which in this case has a size of 3.0×4.3 mas. The dynamic range is 144. The contours in both panels start at $180 \mu\text{Jy}$ and increase by factors of two.

Because VLBI observations involve telescopes at widely separated locations (and can belong to different institutions), VLBI observations are fully automated. The entire “observing run” (a typical VLBI observations lasts around 12 h) including setting up the electronics, driving the antenna to the desired coordinates and recording the raw antenna data on tape or disk, is under computer control and requires no interaction by the observer. VLBI observations generally are supervised by telescope operators, not astronomers.

It should be obvious that each antenna needs to point towards the direction of the source to be observed, but as VLBI arrays are typically spread over thousands of kilometres, a source which just rises at one station can be in transit at another². Then the electronics need to be set up, which involves a very critical step: tuning the local oscillator. In radio astronomy, the signal received by the antenna is amplified many times (in total the signal is amplified by factors of the order of 10^8 to 10^{10}), and to avoid receiver instabilities the signal is “mixed down” to much lower frequencies after the first amplification. The mixing involves injecting a locally generated signal (the local oscillator, or LO, signal) into the signal path with a frequency close to the observing frequency. This yields the signal at a frequency which is the difference between the observing frequency and the LO frequency (see, e.g., Rohlfs 1986 for more details). The LO frequency must be extremely stable (1 part in 10^{15} per day or better) and accurately known (to the sub-Hz level) to ensure that all antennas observe at the same frequency. Interferometers with connected elements such as the VLA or ATCA only need to generate a single LO the output of which can be sent to the individual stations, and any variation in its frequency will affect all stations equally. This is not possible in VLBI, and so each antenna is equipped with a maser (mostly hydrogen masers) which provides a frequency standard to which the LO is phase-locked. After downconversion, the signal is digitized at the receiver output and either stored on tape or disk, or, more recently, directly sent to the correlator via fast network connections (“eVLBI”).

The correlator is sometimes referred to as the “lens” of VLBI observations, because it produces the visibility measurements from the electric fields sampled at the antennas. The data streams are aligned, appropriate delays and phases introduced and then two operations need to be performed on segments of the data: the cross-multiplication of each pair of stations and a Fourier transform, to go from the temporal domain into the spectral domain. Note that Eq. 3 is strictly valid only at a particular frequency. Averaging in frequency is a source of error, and so the observing band is divided into frequency channels to reduce averaging, and the VLBI measurand is a cross-power spectrum.

The cross-correlation and Fourier transform can be interchanged, and correlator designs exists which carry out the cross-correlation first and then the Fourier transform (the “lag-based”, or “XF”, design such as the MPIfR’s Mark IV correlator and the ATCA correlator), and also vice versa (the “FX” correlator such as the VLBA correlator). The advantages and disadvantages of the two

²This can be neatly observed with the VLBA’s webcam images available at <http://www.vlba.nrao.edu/sites/SITECAM/allsites.shtml>. The images are updated every 5 min.

designs are mostly in technical details and computing cost, and of little interest to the observer once the instrument is built. However, the response to spectral lines is different. In a lag-based correlator the signal is Fourier transformed once after cross-correlation, and the resulting cross-power spectrum is the intrinsic spectrum convolved with the sinc function. In a FX correlator, the input streams of both interferometer elements are Fourier transformed which includes a convolution with the sinc function, and the subsequent cross-correlation produces a spectrum which is convolved with the square of the sinc function. Hence the FX correlator has a finer spectral resolution and lower sidelobes (see Romney 1999).

The vast amount of data which needs to be processed in interferometry observations has always been processed on purpose-built computers (except for the very observations where bandwidths of the order of several hundred kHz were processed on general purpose computers). Only recently has the power of off-the-shelf PCs reached a level which makes it feasible to carry out the correlation in software. Deller et al. (2007) describe a software correlator which can efficiently run on a cluster of PC-architecture computers. Correlation is an “embarrassingly parallel” problem, which can be split up in time, frequency, and by baseline, and hence is ideally suited to run in a cluster environment.

The result of the correlation stage is a set of visibility measurements. These are stored in various formats along with auxiliary information about the array such as receiver temperatures, weather information, pointing accuracy, and so forth. These data are sent to the observer who has to carry out a number of calibration steps before the desired information can be extracted.

2.2 Sources of error in VLBI observations

VLBI observations generally are subject to the same problems as observations with connected-element interferometers, but the fact that the individual elements are separated by hundreds and thousands of kilometres adds a few complications.

The largest source of error in typical VLBI observations are phase errors introduced by the earth’s atmosphere. Variations in the atmosphere’s electric properties cause varying delays of the radio waves as they travel through it. The consequence of phase errors is that the measured flux of individual visibilities will be scattered away from the correct locations in the image, reducing the SNR of the observations or, in fact, prohibiting a detection at all. Phase errors arise from tiny variations in the electric path lengths from the source to the antennas. The bulk of the ionospheric and tropospheric delays is compensated in correlation using atmospheric models, but the atmosphere varies on very short timescales so that there are continuous fluctuations in the measured visibilities.

At frequencies below 5 GHz changes in the electron content (TEC) of the ionosphere along the line of sight are the dominant source of phase errors. The ionosphere is the uppermost part of the earth’s atmosphere which is ionised by the sun, and hence undergoes diurnal and seasonal changes. At low GHz frequencies the ionosphere’s plasma frequency is sufficiently close to the observ-

ing frequency to have a noticeable effect. Unlike tropospheric and most other errors, which have a linear dependence on frequency, the impact of the ionosphere is proportional to the inverse of the frequency squared, and so fades away rather quickly as one goes to higher frequencies. Whilst the TEC is regularly monitored³ and the measurements can be incorporated into the VLBI data calibration, the residual errors are still considerable.

At higher frequencies changes in the tropospheric water vapour content have the largest impact on radio interferometry observations. Water vapour⁴ does not mix well with air and thus the integrated amount of water vapour along the line of sight varies considerably as the wind blows over the antenna. Measuring the amount of water vapour along the line of sight is possible and has been implemented at a few observatories (Effelsberg, CARMA, Plateau de Bure), however it is difficult and not yet regularly used in the majority of VLBI observations.

Compact arrays generally suffer less from atmospheric effects because most of the weather is common to all antennas. The closer two antennas are together, the more similar the atmosphere is along the lines of sight, and the delay difference between the antennas decreases.

Other sources of error in VLBI observations are mainly uncertainties in the geometry of the array and instrumental errors. The properties of the array must be accurately known in correlation to introduce the correct delays. As one tries to measure the phase of an electromagnetic wave with a wavelength of a few centimetres, the array geometry must be known to a fraction of that. And because the earth is by no means a solid body, many effects have to be taken into account, from large effects like precession and nutation to smaller effects such as tectonic plate motion, post-glacial rebound and gravitational delay. For an interesting and still controversial astrophysical application of the latter, see Fomalont and Kopeikin (2003). For a long list of these effects including their magnitudes and timescales of variability, see Walker (1999).

2.3 The problem of phase calibration: self-calibration

Due to the aforementioned errors, VLBI visibilities directly from the correlator will never be used to make an image of astronomical sources. The visibility phases need to be calibrated in order to recover the information about the source's location and structure. However, how does one separate the unknown source properties from the unknown errors introduced by the instrument and atmosphere? The method commonly used to do this is called self-calibration and works as follows.

In simple words, in self-calibration one uses a model of the source (if a model is not available a point source is used) and tries to find phase corrections for the antennas to make the visibilities comply with that model. This won't work perfectly unless the model was a perfect representation of the source, and there will be residual, albeit smaller, phase errors. However the corrected

³<http://iono.jpl.nasa.gov>

⁴note that clouds do not primarily consist of water vapour, but of condensated water in droplets.

visibilities will allow one to make an improved source model, and one can find phase corrections to make the visibilities comply with that improved model, which one then uses to make an even better source model. This process is continued until convergence is reached.

The assumption behind self-calibration is that the errors in the visibility phases, which are baseline-based quantities, can be described as the result of antenna-based errors. Most of the errors described in Sec 2.2 are antenna-based: e.g. delays introduced by the atmosphere, uncertainties in the location of the antennas, and drifts in the electronics all are antenna-based. The phase error of a visibility is the combination of the antenna-based phase errors⁵. Since the number of unknown station phase errors is less than the number of visibilities, there is additional phase information which can be used to determine the source structure.

However, self-calibration contains some traps. The most important is making a model of the source which is usually accomplished by making a deconvolved image with the CLEAN algorithm. If a source has been observed during an earlier epoch and the structural changes are expected to be small, then one can use an existing model for a start. If in making that model one includes components which are not real (e.g., by cleaning regions of the image which in fact do not contain emission) then they will be included in the next iteration of self-calibration and will re-appear in the next image. Although it is not easy to generate fake sources or source parts which are strong, weaker source structures are easily affected. The authors have witnessed a radio astronomy PhD student producing a map of a colleague’s name using a data set of pure noise, although the SNR was of the order of only 3.

It is also important to note that for self-calibration the SNR of the visibilities needs to be of the order of 5 or higher within the time it takes the fastest error component to change by a few tens of degrees (“atmospheric coherence time”) (Cotton 1995). Thus the integration time for self-calibration usually is limited by fluctuations in the tropospheric water vapour content. At 5 GHz, one may be able to integrate for 2 min without the atmosphere changing too much, but this can drop to as little as 30 s at 43 GHz. Because radio antennas used for VLBI are less sensitive at higher frequencies observations at tens of GHz require brighter and brighter sources to calibrate the visibility phases. Weak sources well below the detection threshold within the atmospheric coherence time can only be observed using phase referencing (see Sec. 2.3.1).

Another boundary condition for successfully self-calibration is that for a given number of array elements the source must not be too complex. The more antennas, the better because the ratio of number of constraints to number of antenna gains to be determined goes as $N/2$ (The number of constraints is the number of visibilities, $N(N-1)/2$. The number of gains is the number of stations, N , minus one, because the phase of one station is a free parameter and set to zero). Thus self-calibration works very well at the VLA, even with

⁵Baseline-based errors exist, too, but are far less important, see Cornwell and Fomalont (1999) for a list.

complex sources, whereas for an east-west interferometer with few elements such as the ATCA, self-calibration is rather limited. In VLBI observations, however, the sources are typically simple enough to make self-calibration work even with a modest number ($N > 5$) of antennas.

2.3.1 Phase referencing

It is possible to obtain phase-calibrated visibilities without self-calibration by measuring the phase of a nearby, known calibrator. The assumption is that all errors for the calibrator and the target are sufficiently similar to allow calibration of the target with phase corrections derived from the calibrator. While this assumption is justified for the more slowly varying errors such as clock errors and array geometry errors (provided target and calibrator are close), it is only valid under certain circumstances when atmospheric errors are considered. The critical ingredients in phase referencing observations are the target-calibrator separation and the atmospheric coherence time. The separation within which the phase errors for the target and calibrator are considered to be the same is called the isoplanatic patch, and is of the order of a few degrees at 5 GHz. The switching time must be shorter than the atmospheric coherence time to prevent undersampling of the atmospheric phase variations. At high GHz frequencies this can result in observing strategies where one spends half the observing time on the calibrator.

Phase-referencing not only allows one to observe sources too weak for self-calibration, but it also yields precise astrometry for the target relative to the calibrator. A treatment of the attainable accuracy can be found in Pradel et al. (2006).

2.4 Polarization

The polarization of radio emission can yield insights into the strength and orientation of magnetic fields in astrophysical objects and the associated foregrounds. As a consequence and because the calibration has become easier and more streamlined it has become increasingly popular in the past 10 years to measure polarization.

Most radio antennas can record two orthogonal polarizations, conventionally in the form of dual circular polarization. In correlation, one can correlate the right-hand circular polarization signal (RCP) of one antenna with the left-hand circular polarization (LCP) of another and vice versa, to obtain the cross-polarization products RL and LR . The parallel-hand circular polarization cross-products are abbreviated as RR and LL . The four correlation products are converted into the four Stokes parameters in the following way:

$$\begin{aligned}
I &= \frac{1}{2}(RR + LL) \\
Q &= \frac{1}{2}(RL + LR) \\
U &= j\frac{1}{2}(LR - RL) \\
V &= \frac{1}{2}(RR - LL).
\end{aligned}
\tag{5}$$

From the Stokes images one can compute images of polarized intensity and polarization angle.

Most of the calibration in polarization VLBI observations is identical to conventional observations, where one either records only data in one circular polarization or does not form the cross-polarization data at the correlation stage. However, two effects need to be taken care of, the relative phase relation between RCP and LCP and the leakage of emission from RCP and LCP into the cross-products.

The relative phase orientation of RCP and LCP needs to be calibrated to obtain the absolute value for the electric vector position angle (EVPA) of the polarized emission in the source. This is usually accomplished by observing a calibrator which is known to have a stable EVPA with a low-resolution instrument such as a single dish telescope or a compact array.

Calibration of the leakage is more challenging. Each radio telescope has polarization impurities arising from structural asymmetries and errors in manufacturing, resulting in “leakage” of emission from one polarization to the other. The amount of leakage typically is of the order of a few percent and thus is of the same order as the typical degree of polarization in the observed sources and so needs to be carefully calibrated. The leakage is a function of frequency but can be regarded as stable over the course of a VLBI observation.

Unfortunately, sources which are detectable with VLBI are extremely small and hence mostly variable. It is therefore not possible to calibrate the leakage by simply observing a polarization calibrator, and the leakage needs to be calibrated by every observer. At present the calibration scheme exploits the fact that the polarized emission arising from leakage does not change its position angle in the course of the observations. The EVPA of the polarized emission coming from the source, however, will change with respect to the antenna and its feed horns, because most antennas have alt-azimuth mounts and so the source seems to rotate on the sky as the observation progresses⁶. One can think of this situation as the sum of two vectors, where the instrumental polarization is a fixed vector and the astronomical polarization is added to this vector and rotates during the observation. Leakage calibration is about separating these two contributions, by observing a strong source at a wide range of position

⁶The 26m antenna at the Mount Pleasant Observatory near Hobart, Australia, has a parallactic mount and thus there is no field rotation.

angles. The method is described in Leppänen et al. (1995), and a more detailed treatment of polarization VLBI is given by Kembell (1999).

2.5 Spectral line VLBI

In general a set of visibility measurements consists of cross-power spectra. If a continuum source has been targeted, the number of spectral points is commonly of the order of a few tens. If a spectral line has been observed, the number of channels can be as high as a few thousand, and is limited by the capabilities of the correlator. The high brightness temperatures (Section 3.1.3) needed to yield a VLBI detection restrict observations to masers, or relatively large absorbers in front of non-thermal continuum sources. The setup of frequencies requires the same care as for short baseline interferometry, but an additional complication is that the antennas have significant differences in their Doppler shifts towards the source. See Westpfahl (1999), Rupen (1999), and Reid et al. (1999) for a detailed treatment of spectral-line interferometry and VLBI.

2.6 Pulsar gating

If pulsars are to be observed with a radio interferometer it is desirable to correlate only those times where a pulse is arriving (or where it is absent, Stappers et al. 1999). This is called pulsar gating and is an observing mode available at most interferometers.

2.7 Wide-field limitations

The equations in Sec 2.1 are strictly correct only for a single frequency and single points in time, but radio telescopes must observe a finite bandwidth, and in correlation a finite integration time must be used, to be able to detect objects. Hence a point in the (u, v) plane always represents the result of averaging across a bandwidth, $\Delta\nu$, and over a time interval, $\Delta\tau$ (the *points* in Fig. 2 actually represent a continuous frequency band in the radial direction and a continuous observation in the time direction).

The errors arising from averaging across the bandwidth are referred to as bandwidth smearing, because the effect is similar to chromatic aberration in optical systems, where the light from one single point of an object is distributed radially in the image plane. In radio interferometry, the images of sources away from the observing centre are smeared out in the radial direction, reducing the signal-to-noise ratio. The effect of bandwidth smearing increases with the fractional bandwidth, $\Delta\nu/\nu$, the square root of the distance to the observing centre, $\sqrt{l^2 + m^2}$, and with $1/\theta_b$, where θ_b is the FWHM of the synthesized beam. Interestingly, however, the dependencies of ν of the fractional bandwidth and of θ_b cancel one another, and so for any given array and bandwidth, bandwidth smearing is independent of ν (see Thompson et al. 2001). The effect can be avoided if the observing band is subdivided into a sufficiently large number of frequency channels for all of which one calculates the locations in the (u, v) plane

separately. This technique is sometimes deliberately chosen to increase the (u, v) coverage, predominantly at low frequencies where the fractional bandwidth is large. It is then called multi-frequency synthesis.

By analogy, the errors arising from time averaging are called time smearing, and they smear out the images approximately tangentially to the (u, v) ellipse. It occurs because each point in the (u, v) plane represents a measurement during which the baseline vector rotated through $\omega_E \Delta\tau$, where ω_E is the angular velocity of the earth. Time smearing also increases as a function of $\sqrt{l^2 + m^2}$ and can be avoided if $\Delta\tau$ is chosen small enough for the desired field of view.

VLBI observers generally are concerned with fields of view (FOV) of no more than about one arcsecond, and consequently most VLBI observers are not particularly bothered by wide field effects. However, wide-field VLBI has gained momentum in the last few years as the computing power to process finely time- and bandwidth-sampled data sets has become widely available. Recent examples of observations with fields of view of $1'$ or more are reported on in McDonald et al. (2001), Garrett et al. (2001), Garrett et al. (2005), Lenc and Tingay (2006) and Lenc et al. (2006). The effects of primary beam attenuation, bandwidth smearing and time smearing on the SNR of the observations can be estimated using the calculator at <http://astronomy.swin.edu.au/~elenc/Calculators/wfcalc.php>.

2.8 VLBI at mm wavelengths

In the quest for angular resolution VLBI helps to optimize one part of the equation which approximates the separation of the finest details an instrument is capable of resolving, $\theta = \lambda/D$. In VLBI, D approaches the diameter of the earth, and larger instruments are barely possible, although “space-VLBI” can extend an array beyond earth. However, it is straightforward to attempt to decrease λ to push the resolution further up.

However, VLBI observations at frequencies above 20 GHz ($\lambda = 15$ mm) become progressively harder towards higher frequencies. Many effects contribute to the difficulties at mm wavelengths: the atmospheric coherence time is shorter than one minute, telescopes are less efficient, receivers are less sensitive, sources are weaker than at cm wavelengths, and tropospheric water vapour absorbs the radio emission. All of these effects limit mm VLBI observations to comparatively few bright continuum sources or sources hosting strong masers. Hence also the number of possible phase calibrators for phase referencing drops. Nevertheless VLBI observations at 22 GHz (13 mm), 43 GHz ($\lambda \approx 7$ mm) and 86 GHz ($\lambda \approx 3$ mm) are routinely carried out with the world’s VLBI arrays. For example, of all projects observed in 2005 and 2006 with the VLBA, 16 % were made at 22 GHz, 23 % at 43 GHz, and 4 % at 86 GHz⁷.

Although observations at higher frequencies are experimental, a convincing demonstration of the feasibility of VLBI at wavelengths shorter than 3 mm was made at 2 mm (147 GHz) in 2001 and 2002 (Greve et al. 2002, Krichbaum et al. 2002a). These first 2 mm-VLBI experiments resulted in detections of about one

⁷e.g., <ftp://ftp.aoc.nrao.edu/pub/cumvlbaobs.txt>

dozen quasars on the short continental and long transatlantic baselines (Krichbaum et al. 2002a). In an experiment in April 2003 at 1.3 mm (230 GHz) a number of sources was detected on the 1150 km long baseline between Pico Veleta and Plateau de Bure (Krichbaum et al. 2004). On the $6.4 \text{ G} \lambda$ long transatlantic baseline between Europe and Arizona, USA fringes for the quasar 3C454.3 were clearly seen. This detection marks a new record in angular resolution in Astronomy (size $< 30 \mu\text{as}$). It indicates the existence of ultra compact emission regions in AGN even at the highest frequencies (for 3C454.3 at $z=0.859$, the rest frame frequency is 428 GHz). So far, no evidence for a reduced brightness temperature of the VLBI-cores at mm wavelengths was found (Krichbaum et al. 2004). These are the astronomical observations with the highest angular resolution possible today at any wavelength.

2.9 The future of VLBI: eVLBI, VLBI in space, and the SKA

One of the key drawbacks of VLBI observations has always been that the raw antenna signals are recorded and the visibilities formed only later when the signals are combined in the correlator. Thus there has never been an immediate feedback for the observer, who has had to wait several weeks or months until the data are received for investigation. With the advent of fast computer networks this has changed in the last few years. First small pieces of raw data were sent from the antennas to the correlator, to check the integrity of the VLBI array, then data were directly streamed onto disks at the correlator, then visibilities were produced in real-time from the data sent from the antennas to the correlator. A brief description of the transition from tape-based recording to real-time correlation of the European VLBI Network (EVN) is given in Szomoru et al. (2004). The EVN now regularly performs so-called “eVLBI” observing runs which is likely to be the standard mode of operation in the near future. The Australian Long Baseline Array (LBA) completed a first eVLBI-only observing run in March 2007⁸.

It has been indicated in Sec. 2.8 that resolution can be increased not only by observing at higher frequencies with ground-based arrays but also by using a radio antenna in earth orbit. This has indeed been accomplished with the Japanese satellite “HALCA” (Highly Advanced Laboratory for Communications and Astronomy, Hirabayashi et al. 2000) which was used for VLBI observations at 1.6 GHz, 5 GHz and 22 GHz (albeit with very low sensitivity) between 1997 and 2003. The satellite provided the collecting area of an 8 m radio telescope and the sampled signals were directly transmitted to ground-based tracking stations. The satellite’s elliptical orbit provided baselines between a few hundred km and more than 20 000 km, yielding a resolution of up to 0.3 mas (Dodson et al. 2006, Edwards and Piner 2002). Amazingly, although HALCA only provided left-hand circular polarization, it has been used successfully to observe polarized emission (e.g., Bach et al. 2006a, Kembell et al. 2000). But this was only possible because

⁸<http://www.atnf.atnf.csiro.au/vlbi/evlbi>

the ground array observed dual circular polarization. Many of the scientific results from VSOP are summarized in two special issues of Publications of the Astronomical Society of Japan (PASJ, Vol. 52, No. 6, 2000 and Vol. 58, No. 2, 2006). The successor to HALCA, ASTRO-G, is under development and due for launch in 2012. It will have a reflector with a diameter of 9 m and receivers for observations at 8 GHz, 22 GHz, and 43 GHz.

The Russian mission RadioAstron is a similar project to launch a 10 m radio telescope into a high apogee orbit. It will carry receivers for frequencies between 327 MHz and 25 GHz, and is due for launch in October 2008.

The design goals for the Square Kilometre Array (SKA), a large, next-generation radio telescope built by an international consortium, include interferometer baselines of at least 3000 km. At the same time, the design envisions the highest observing frequency to be 25 GHz, and so one would expect a maximum resolution of around 1 mas. However, most of the baselines will be shorter than 3000 km, and so a weighted average of all visibilities will yield a resolution of a few mas, and of tens of mas at low GHz frequencies. The SKA's resolution will therefore be comparable to current VLBI arrays. Its sensitivity, however, will be orders of magnitude higher (sub- μ Jy in 1 h). The most compelling consequence of this is that the SKA will allow one to observe thermal sources with brightness temperatures of the order of a few hundred Kelvin with a resolution of a few mas. Current VLBI observations are limited to sources with brightness temperatures of the order of 10^6 K and so to non-thermal radio sources and coherent emission from masers. With the SKA one can observe star and black hole formation throughout the universe, stars, water masers at significant redshifts, and much more. Whether or not the SKA can be called a VLBI array in the original sense (an array of isolated antennas the visibilities of which are produced later on) is a matter of taste: correlation will be done in real time and the local oscillator signals will be distributed from the same source. Still, the baselines will be "very long" when compared to 20th century connected-element interferometers. A short treatment of "VLBI with the SKA" can be found in Carilli (2005). Comprehensive information about the current state of the SKA is available on the aforementioned web page; prospects of the scientific outcomes of the SKA are summarized in Carilli and Rawlings (2004); and engineering aspects are treated in Hall (2005).

2.10 VLBI arrays around the world and their capabilities

This section gives an overview of presently active VLBI arrays which are available for all astronomers and which are predominantly used for astronomical observations. Antennas of these arrays are frequently used in other array's observations, to either add more long baselines or to increase the sensitivity of the observations. Joint observations including the VLBA and EVN antennas are quite common; also observations with the VLBA plus two or more of the phased VLA, the Green Bank, Effelsberg and Arecibo telescopes (then known as the High Sensitivity Array) have recently been made easier through a common application process. Note that each of these four telescopes has more collecting

area than the VLBA alone, and hence the sensitivity improvement is considerable.

Table 1: VLBI telescope information on the World Wide Web.

Square Kilometre Array	http://www.skatelescope.org
High Sensitivity Array	http://www.nrao.edu/HSA
European VLBI Network	http://www.evlbi.org
Very Long Baseline Array	http://www.vlba.nrao.edu
Long Baseline Array	http://www.atnf.csiro.au/vlbi
VERA	http://veraserver.mtk.nao.ac.jp/outline/index-e.html
GMVA	http://www.mpi-fr-bonn.mpg.de/div/vlbi/globalmm

2.10.1 The European VLBI Network (EVN)

The EVN is a collaboration of 14 institutes in Europe, Asia, and South Africa and was founded in 1980. The participating telescopes are used in many independent radio astronomical observations, but are scheduled three times per year for several weeks together as a VLBI array. The EVN provides frequencies in the range of 300 MHz to 43 GHz, though due to its inhomogeneity not all frequencies can be observed at all antennas. The advantage of the EVN is that it includes several relatively large telescopes such as the 76 m Lovell telescope, the Westerbork array, and the Effelsberg 100 m telescope, which provide high sensitivity. Its disadvantages are a relatively poor frequency agility during the observations, because not all telescopes can change their receivers at the flick of a switch. EVN observations are mostly correlated on the correlator at the Joint Institute for VLBI in Europe (JIVE) in Dwingeloo, the Netherlands, but sometimes are processed at the Max-Planck-Institute for Radio Astronomy in Bonn, Germany, or the National Radio Astronomy Observatory in Socorro, USA.

2.10.2 The U.S. Very Long Baseline Array (VLBA)

The VLBA is a purpose-built VLBI array across the continental USA and islands in the Caribbean and Hawaii. It consists of 10 identical antennas with a diameter of 25 m, which are remotely operated from Socorro, New Mexico. The VLBA was constructed in the early 1990s and began full operations in 1993. It provides frequencies between 300 MHz and 86 GHz at all stations (except two which are not worth equipping with 86 GHz receivers due to their humid locations). Its advantages are excellent frequency agility and its homogeneity, which makes it very easy to use. Its disadvantages are its comparatively small antennas, although the VLBA is frequently used in conjunction with the phased VLA and the Effelsberg and Green Bank telescopes.

2.10.3 The Australian Long Baseline Array (LBA)

The LBA consists of six antennas in Ceduna, Hobart, Parkes, Mopra, Narrabri, and Tidbinbilla. Like the EVN it has been formed from existing antennas and so the array is inhomogeneous. Its frequency range is 1.4 GHz to 22 GHz, but not all antennas can observe at all available frequencies. Stretched out along Australia's east coast, the LBA extends in a north-south direction which limits the (u, v) coverage. Nevertheless, the LBA is the only VLBI array which can observe the entire southern sky, and the recent technical developments are remarkable: the LBA is at the forefront of development of eVLBI and at present is the only VLBI array correlating all of its observations using the software correlator developed by Deller et al. (2007) on a computer cluster of the Swinburne Centre for Astrophysics and Supercomputing.

2.10.4 The Korean VLBI Network (KVN)

The KVN is a dedicated VLBI network consisting of three antennas which currently is under construction in Korea. It will be able to observe at up to four widely separated frequencies (22 GHz, 43 GHz, 86 GHz, and 129 GHz), but will also be able to observe at 2.3 GHz and 8.4 GHz. The KVN has been designed to observe H_2O and SiO masers in particular and can observe these transitions simultaneously. Furthermore, the antennas can slew quickly for improved performance in phase-referencing observations.

2.10.5 The Japanese VERA network

VERA (VLBI Exploration of Radio Astrometry) is a purpose-built VLBI network of four antennas in Japan. The scientific goal is to measure the annual parallax towards galactic masers (H_2O masers at 22 GHz and SiO masers at 43 GHz), to construct a map of the Milky Way. Nevertheless, VERA is open for access to carry out any other observations. VERA can observe two sources separated by up to 2.2° simultaneously, intended for an extragalactic reference source and for the galactic target. This observing mode is a significant improvement over the technique of phase-referencing where the reference source and target are observed in turn. The positional accuracy is expected to reach $10 \mu\text{as}$, and recent results seem to reach this (Hirota et al. 2007b). VERA's frequency range is 2.3 GHz to 43 GHz.

2.10.6 The Global mm-VLBI Array (GMVA)

The GMVA is an inhomogeneous array of 13 radio telescopes capable of observing at a frequency of 86 GHz. Observations with this network are scheduled twice a year for about a week. The array's objective is to provide the highest angular resolution on a regular schedule.

3 Astrophysical applications

High resolution radio observations are used in many astronomical fields. They provide information about the structures around Active Galactic Nuclei (AGN), their accretion disks, powerful relativistic jets, magnetic fields, and absorbing material, and they are used to image peculiar binary stars, radio-stars and young supernova remnants. Spectroscopic VLBI-observations allow one to investigate compact maser emitting regions of various kinds in galaxies, star birth regions and stellar envelopes. The phase-referencing technique allows to determine source positions with highest possible accuracy. This section will summarize some of the observational highlights obtained by very long baseline radio interferometers.

3.1 Active Galactic Nuclei and their jets

The luminosity of most of the known galaxies is dominated in the optical by their stellar emission, but in some galaxies a significant fraction of the energy output has a non-thermal origin. These are called active galaxies or Active Galactic Nuclei (AGN), if the non-thermal emission comes mainly from the core. Although AGN represent only a small fraction of all galaxies they have been studied intensively over the last 40 years at all accessible wavelengths. This is partly because their high luminosities made them the only objects that could be studied at cosmologically significant distances for a long time. At radio wavelength some active galaxies are the most luminous sources in the sky and were the first sources detected in the early days of radio astronomy (e.g. Baade and Minkowski 1954).

In many powerful radio galaxies, the radio emission is detected several hundreds of kiloparsec away from the centre of the associated optical galaxy (e.g. Bridle and Perley 1984, and references therein). These regions are called radio lobes. In other cases, however, a large portion of the radio emission comes from much smaller regions at the centre of the galaxy with dimensions of only a few parsecs. These centres are also visible in lobe-dominated objects, and they supply the lobes with plasma via relativistic outflows, which are called jets.

Since single-dish radio telescopes have rather low resolution, observations of jets and lobes in radio galaxies were one of the main drivers for the development of radio interferometers in the early 1960s (Ryle and Hewish 1960). In particular the development of Very Long Baseline Interferometry (VLBI) made it possible to image the inner regions of AGN and it is still the only technique capable to image sub-parsec-scale structures in extra-galactic objects. The direct imaging of parsec-scale jets and the complementary study of activity in the associated AGN in all spectral regimes has broadly enhanced our understanding of these objects. Based on the last decades of detailed observations of AGN a common scheme about their nature has been established.

3.1.1 The AGN paradigm

It is believed that the high luminosities of AGN are due to accretion on to a super-massive black hole (e.g. Begelman et al. 1984, Meier et al. 2001). The $10^6-10^9 M_\odot$ black hole is surrounded by an accretion disc and probably a hot corona mainly radiating at optical to soft X-ray energies (Antonucci and Miller 1985). In the vicinity of the nucleus high velocity gas, characterized by broad optical emission lines, forms the so called broad-line region (BLR), and lower velocity gas with narrower emission lines forms the narrow-line region (NLR). An obscuring torus of gas and dust is hiding the central region including the BLR from some directions. The term “torus” is often used in this context, but it is not sure at all which geometrical form the absorber has. At the poles relativistic jets are formed and expand for several tens of kiloparsec or even up to megaparsecs (e.g. Urry and Padovani 1995).

Not all AGN show observational signatures of every component. Therefore several classes were defined that divide AGN mainly into type 1 source which exhibit broad emission lines from the BLR and type 2 sources that do not show broad emission lines. Both groups contain radio-loud and radio-quiet objects, with a division being made at a ratio of the 5 GHz radio to the optical R -band flux of 10 (see also Sect. 3.1.4). Table 2 summarizes the separation into different types of AGN. Type 0 sources are called blazars and originally defined sources with no line emission. This class mainly contains BL Lac objects and flat spectrum quasars (FSRQs). However, with modern and more sensitive observations emission lines have been detected in several FSRQs and also in a few BL Lac objects. Narrow line radio galaxies include two radio morphology types: the lower-luminosity Fanaroff-Riley type I (FRI) radio galaxies with often symmetrical jets that broaden and fade away from the nucleus, and the FRII radio galaxies, which show highly collimated jets leading to well-defined lobes with hot spots (Fanaroff and Riley 1974).

Table 2: Properties of AGN (see text for details).

Radio loudness	Emission line properties		
	Type 2 narrow lines	Type 1 broad lines	Type 0 “no” lines
radio-quiet:	Seyfert 2 Liners	Seyfert 1 Quasar	
radio-loud:	NLRG	Quasar	Blazars

Obscuring material found in type 2 sources (Rowan-Robinson 1977) and the detection of polarized broad emission lines in Seyfert 2 galaxies (Antonucci and Miller 1985) led to the idea of a unified scheme for AGN. In addition, depending on the orientation of the jet to our line of sight, relativistic beaming (see Sect. 3.1.3 about relativistic beaming) of the jet emission strongly affects the appearance and classification of the AGN. Whether AGN are classified type 1 or 2 depends on the obscuration of the luminous nucleus, and whether a

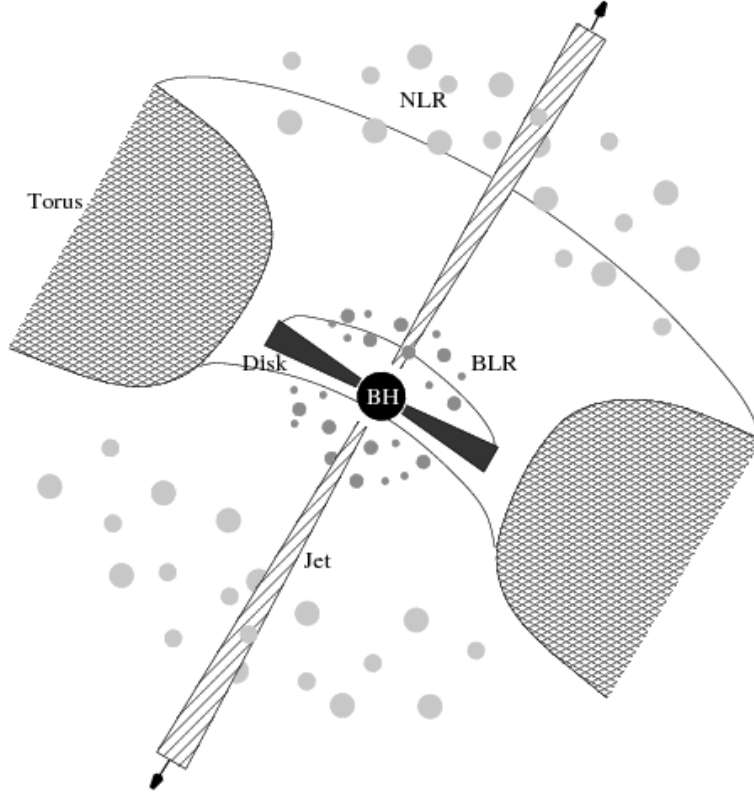


Figure 5: Unification scheme for AGN (not to scale). In this picture the appearance of an AGN depends strongly on the viewing angle. For some directions the central part is hidden by the torus (or an absorber of some other geometrical form), whereas from other directions the innermost parts are visible.

radio-loud AGN is a blazar or a radio galaxy depends on the angle between the relativistic jet and the line of sight (e.g. Antonucci 1993, Urry and Padovani 1995). An illustration of the unified scheme for AGN is given in Fig. 5.

3.1.2 VLBI structures in AGN jets

AGN are in the focus of VLBI observations since the first measurements were performed in 1967. At the beginning of VLBI mainly detailed studies of a few bright sources were carried out, but as new technical developments increased the observed bandwidth and therefore the sensitivity of the observations, and with the advent of the VLBA, larger surveys of hundreds of sources for statistical studies became possible (Fomalont et al. 2000, Kellermann et al. 1998, Lister and Homan 2005, Pearson and Readhead 1988, Taylor et al. 1996). Newer surveys even provide total intensity and linear polarization images of more than

1000 sources (Beasley et al. 2002, Helmboldt et al. 2007).

When speaking about relativistic jets in AGN one usually only considers radio-loud AGN, because they harbour the brightest, largest, and best studied jets. Nevertheless, they constitute only about 10 % of the AGN population and it seems likely that also radio-quiet AGN produce jets (e.g. Falcke et al. 1996a;b, Ulvestad et al. 2005). The formation of powerful jets may depend on many parameters, but given the number of different types of objects from AGN to stellar black holes and Herbig-Haro objects, where jets have been observed, jet formation must be possible in almost all circumstances.

The typical parsec-scale radio morphology of a radio-loud AGN is a bright point-like component, referred to as the “core” component, and an extension pointing away from the core: the jet (Fig. 6, top panels). This class makes up about 90 % of the radio-loud AGN. The rest divides into point-like or double-sided source (Fig. 6, bottom panels) or more irregular sources. In the case of the point-like sources we probably see only the core, but for the others it is sometimes more difficult to judge which component the core is. Usually this is done on the bases of compactness and the radio spectrum. The core has a flat to inverted radio spectrum ($\alpha > -0.5$ with $S \propto \nu^\alpha$). Since the synchrotron spectrum should be flat only at its peak frequency the appearance of flat spectra in AGN cores over a wide range of frequencies caused some discussion (e.g. Marscher 1977). There is still some discussion about this, but the most common explanation is that the flat core spectrum is the result of a superposition of several distinct synchrotron components each of which has a peaked spectrum at a slightly different frequency (“cosmic conspiracy”, Cotton et al. 1980). The jets have usually steeper spectra with $\alpha < -0.7$, resulting from optically thin synchrotron emission.

In many aspects the appearance of radio-quiet objects is similar to their radio-loud counterparts. However, extended jet structures are rare and besides the core only some distinct jet components are visible (e.g. Falcke 2001, Nagar et al. 2002, Ulvestad et al. 2005). The appearance of parts of the jet and the observations of multiple bend in the jets of Seyfert galaxies might be explained be the interaction of the jet with NLR or BLR clouds (e.g. Middelberg et al. 2007, Mundell et al. 2003).

A comparison between the VLBI images in Fig. 6 and the sketch of an AGN in Fig. 5 is not always straightforward. The jet in Fig. 6 (top panel) might be easy to identify, however, the “core” for example does not correspond to the central engine, but usually marks the transition region of optically thick to thin emission (Königl 1981). Since the location of this transition zone depends on the observing frequency, the apparent location of the core moves towards the central engine at higher frequencies, which has been observed in some sources (Lobanov 1998b, Marscher 2005b). Other possibilities are that the core is a conical “re-collimation” shock that accelerates particles (Bogovalov and Tsinganos 2005, Daly and Marscher 1988, Gomez et al. 1995) or the jet initially is not well aligned with the line of sight, but changes its direction towards the observer so that the beaming factor increases and the jet becomes visible. The formation of the jet itself takes place presumably on scales of a few 10 to 1000 Schwarzschild

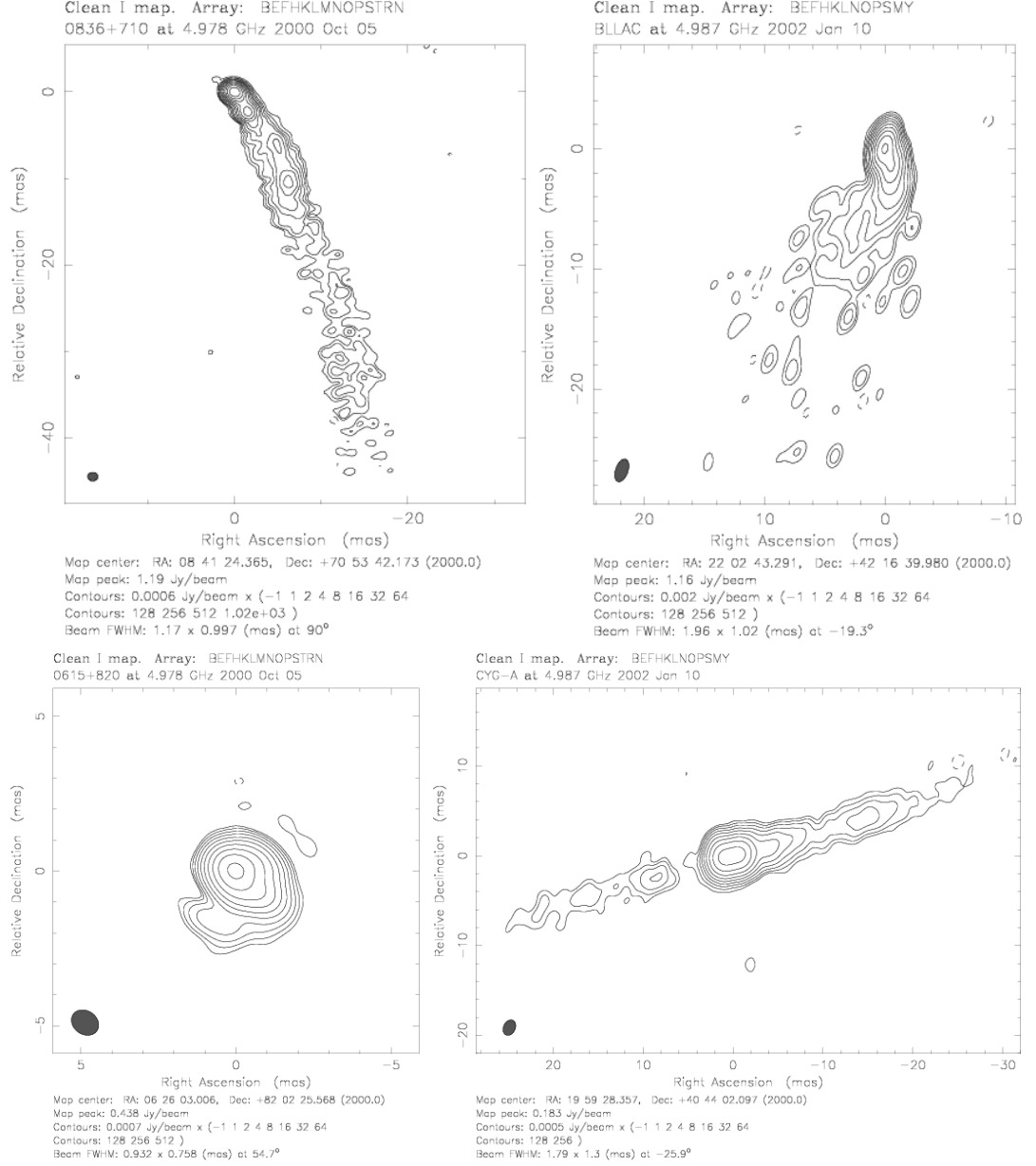


Figure 6: Typical parsec-scale radio morphology of AGN seen at 5 GHz using the VLBA plus Effelsberg. 90 % of the sources show this core-jet structure with smooth parts, knots, bends or gaps (top panels). Some are quasi point-like (bottom-left), or, if the viewing angle is large enough, show double sided jets (bottom-right).

radii ($R_S = 2GM/c^2$). The Schwarzschild radius of a typical AGN black hole of $10^8 M_\odot$ is of the order of 2 AU (3×10^{12} m, $R_S \approx 3000 m_{\frac{M}{M_\odot}}$).

The closest look so far into the central engine of an AGN was obtained with global VLBI observations of M87 at 43 GHz and 86 GHz (Junor et al. 1999, Krichbaum et al. 2006, Ly et al. 2007). M87 is an E0 galaxy at the centre of the Virgo cluster, and has one of the nearest extragalactic jets. Together with its large inferred black hole mass of $3 \times 10^9 M_\odot$ (e.g. Macchetto et al. 1997, and references therein), M87 is an ideal candidate for jet formation studies. At a distance of 14.7 Mpc, 1 mas corresponds to a linear scale of 0.071 pc and the Schwarzschild radius of the black hole is about 60 AU, corresponding to 0.0003 pc. Surprisingly, this is very similar to the linear resolution in Sgr A*⁹. The observations revealed that the jet in M87 starts fairly broad at an opening angle of 60° on scales < 0.5 mas (0.04 pc), but collimates to about 5° within the first few parsecs (e.g., Kovalev et al. 2007, Ly et al. 2007). Together with the slow proper motion in the parsec-scale jet (Biretta et al. 1995, Reid et al. 1989), this supports the idea of a magnetically dominated launching of the jet with a long collimation and acceleration zone (Vlahakis and Königl 2004). In its initial phase (ultra compact jet) the jet is probably dominated by electromagnetic processes (Meier et al. 2001, Sikora et al. 2005), and is visible as the compact VLBI-core where the jet becomes optically thin for radio emission (Lobanov 1998b, Lobanov and Zensus 1999).

Several other VLBI observations made use of the space-VLBI technique to achieve highest angular resolution, and to resolve prominent quasar jets in the transverse direction (e.g. 3C273: Lobanov and Zensus 2001; 0836+714: Lobanov et al. 2006). This allowed a detailed study of jet propagation and jet internal processes, like i.e. the development of instabilities. In Centaurus A VSOP observations at 5 GHz by Horiuchi et al. (2006) revealed a sub-parsec scale jet-opening and collimation region similar to that observed in M87 at mm wavelengths (Junor et al. 1999, Krichbaum et al. 2006). Although the resolution was not as high as in the case of M87 the observations suggested that the jet collimation takes place on scales of a few $10 R_S$ to $1000 R_S$, which supports MHD disk outflow models (e.g. Meier et al. 2001).

Future space VLBI observations at higher frequencies will provide even higher angular resolution and will probably be able to image the collimation region within $100 R_S$ of the central engine in many more AGN. At 43 GHz, the angular resolution, as it is planned for VSOP 2, will be a few ten micro-arcseconds, closely matching the possible angular resolution of ground based mm-VLBI at 230 GHz. Images obtained at different frequencies and with matched angular resolution, can help to detect spectral and polarization properties of compact regions, which are not observable otherwise (e.g. Gabuzda and Gómez 2001, Papageorgiou et al. 2006, Pushkarev et al. 2005).

An illustration of the structures and emitting regions of the central part of a

⁹M87 is approximately 2000 times more distant than Sgr A* but has a black hole with a mass 1000 greater than Sgr A*'s, so these two effects almost exactly cancel each other when the resolution is measured in Schwarzschild radii.

radio-loud AGN is given in Fig. 7. Observations suggest that the ultra compact jet is dominated by smooth changes in the particle density associated with nuclear flares in the central engine and not with strong shocks (Lobanov 1998a, Lobanov and Zensus 1999). On the other hand parsec-scales shock models (Hughes et al. 1985; 1989, Marscher and Gear 1985) are able to explain the observed flux density and polarization characteristics of jets (Cawthorne 2006, Jorstad et al. 2005, Lister and Homan 2005). Further evidence for shocks comes from observations of rapid changes of the turnover frequency (frequency at the maximum of the synchrotron spectrum) along the jet (Lobanov 1998a).

In several AGN small changes in the jet direction on sub-parsec scales over a period of a few years have been observed (e.g. Biretta et al. 1986, Carrara et al. 1993, Jorstad et al. 2005; 2001a, Stirling et al. 2003). For example, global 3 mm VLBI observations of NRAO 150 revealed an apparent rotation of the inner jet at a rate of up to $\sim 11^\circ$ per year, which is associated with a non-ballistic superluminal motion of the jet within this region and probably would have remained undetected at lower resolution (Agudo et al. 2007).

The most common explanation for this phenomenon is a precessing jet, which could be caused by a binary super-massive black hole system (Biretta et al. 1986, Hummel et al. 1992). Although the observed angles are small ($< 10^\circ$), which translates to less than 1° when deprojected, the time scale is set by the movement of some section of the jet that might not itself move with relativistic velocities. Therefore, the time scale is unaffected by Doppler blueshifting and can lead to rather extreme physical conditions of the nuclear region (Lobanov and Roland 2005). The time scale for the precession of a supermassive black hole is of the order of $\geq 10^4$ years and becomes visible on kiloparsec scales (Gower et al. 1982). However on parsec scales hydrodynamic effects also can lead to a precession of the jet (e.g. Hardee 2003, Hughes et al. 2002). In this case the precession may be introduced by a strong shock at the base of the jet. Observations of more erratic changes in the jet direction (Jorstad et al. 2005) support this idea and indicate that it is not necessarily a regular periodic process.

Further out, on scales of about > 100 pc, the appearance of the jet becomes more and more dominated by instabilities of the jet flow, most importantly Kelvin-Helmholtz instabilities (Lobanov et al. 2003, Lobanov and Zensus 2001, Perucho and Lobanov 2007, Perucho et al. 2006). Since the jets have steep spectra, high resolution at low frequencies is necessary to successfully model the transverse structures using Kelvin-Helmholtz instabilities. Therefore most of those observations were made at a wavelength of 18 cm with the Space VLBI Program, which combines a world array of radio telescopes with the satellite radio antenna HALCA.

A common method to study the emission processes in the inner jet is the combined analysis of light curves from radio to X-rays or even γ -rays with multi-epoch VLBI observations at high frequencies (e.g. Bach et al. 2006b, Jorstad et al. 2001a; 2007, Pyatunina et al. 2006, Savolainen et al. 2002). The comparison of the broad-band variability with structural changes in the radio jet allows to directly identify those regions which are responsible for the variability.

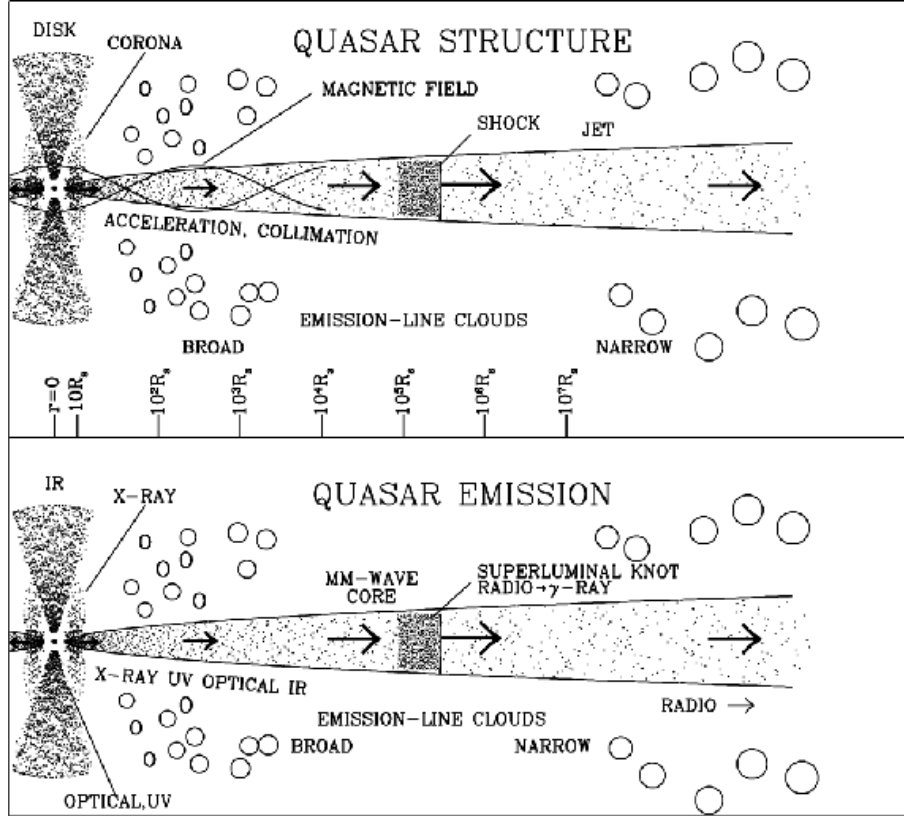


Figure 7: Illustration of the central part of a radio-loud AGN. The density of the dots in the disk, corona, and jet very roughly indicates the density of plasma (top panel) or intensity of emission (bottom panel) in a reference frame in which there is no beaming. Note the logarithmic length scale beyond $10 R_s$, where R_s is the Schwarzschild radius. Only a single superluminal knot is shown; usually there are several (courtesy Marscher 2005a).

The detection of wavelength-dependent time delays further helps to constrain the distances between the various emission regions along the jet. In addition, multi-epoch VLBI observations can be used to measure the jet speed and the source geometry (see Sect. 3.1.3), and the analysis of linear polarization provides information on the magnetic field structure (see Sect. 3.1.6 for more details on VLBI polarimetry).

In more recent observations of 3C 120 the high resolution of global 3 mm VLBI was used in combination with its millimetre-wave continuum spectrum and a computer model to derive the number density of the combined electron-positron population in the core and compact knots in the jet (Marscher et al. 2007). Assuming that the jet contains a pure pair plasma, this density and the efficiency of the eventual annihilation can be used to predict the intensity of the narrow electron-positron annihilation line, which should be detectable with modern high energy satellites.

3.1.3 Brightness temperatures and jet speeds

The brightness temperature, T_B , the physical temperature a blackbody would need to have to produce the observed radio flux density, is defined in analogy with the Rayleigh-Jeans Law as:

$$T_B = \frac{c^2 B_\nu}{2\nu^2 k}, \quad (6)$$

where T_B is given in K, c is the speed of light in m s^{-1} , B_ν is the flux density per unit solid angle, Ω , in $\text{W m}^{-2} \text{Hz}^{-1} \text{sr}^{-1}$, ν is the observing frequency and k the Boltzmann constant in J/K. To convert Eq. 6 into convenient units, Ω can be expressed as the area of a sphere intersected by a cone with opening angle θ , yielding $\Omega = 4\pi \sin^2(\theta/4)$. Using the approximation $\sin(x) \approx x$ for $x \ll 1$ and introducing units of milli-arcseconds, $\Omega = 1.846 \times 10^{-17} \theta$. Converting B_ν and ν to Jy/beam and GHz, respectively, yields

$$T_B = 1.76 \times 10^{12} \frac{S_\nu}{\theta^2 \nu^2}. \quad (7)$$

VLBI core components typically have measured brightness temperatures of 10^{10} K to 10^{12} K, which is well above the limit for thermal emission, and indicates a non-thermal origin such as synchrotron emission from relativistic electrons. However, even the brightness temperature for synchrotron radiation has an upper-limit – the Compton limit. Kellermann and Pauliny-Toth (1969) have shown that for brightness temperatures exceeding 10^{12} K the energy losses due to inverse Compton scattering become dominant and the brightness temperature decreases to values between 10^{11} K to 10^{12} K, where inverse Compton and synchrotron losses are of the same order.

Indeed most of early VLBI experiments showed that the brightness temperatures of nearly all sources falls into the small range of $T_B \approx 10^{11}$ K to $T_B \approx 10^{12}$ K (Kellermann and Pauliny-Toth 1969). However, in the following decades it became clear that this was a natural consequence of the size of the

Earth (longest possible baseline) and the limited range of flux densities observed, and had nothing to do with radio source physics. This is because the resolution of any interferometer is given by $\theta = \lambda/D$ where λ is the wavelength of observation, and D is the baseline length. For a typical radio source with $1 \text{ Jy} < S_\nu < 10 \text{ Jy}$, and a common baseline length $D \sim 5000 \text{ km}$ to 8000 km , T_B will always be 10^{11} K to 10^{12} K (Kellermann 2003).

More recent VLBA (Kellermann et al. 1998, Zensus et al. 2002) and space VLBI observations (e.g. Horiuchi et al. 2004, Tingay et al. 2001) suggest that there are sources in which the maximum observed brightness temperature reaches 10^{13} K or even higher values. In particular IDV sources were found to have considerably higher core brightness temperatures than non-IDV sources (Lister et al. 2001, Tingay et al. 2001), which agrees with the finding that the IDV originates from the VLBI-core component (Bach et al. 2006a). There is evidence that even the majority of the radio-loud AGN have core brightness temperatures above 10^{12} K (Horiuchi et al. 2004). Conversely, a lower limit of T_B of around 10^{5-6} K is given by the limited sensitivity of today's VLBI observations of a few $10 \mu\text{Jy}$ to $100 \mu\text{Jy}$.

The excess of T_B is usually explained in terms of relativistic beaming. If the jet is moving relativistically, relativistic beaming will increase the flux density without changing the size of the jet, hence it will lead to an apparent increase of T_B beyond the allowed value, proportional to the Doppler factor, δ : $T'_B \propto T_B \delta$ with $\delta = [\gamma(1 - \beta \cos \theta)]^{-1}$, where γ is Lorentz factor of the flow, θ is the viewing angle, and $\beta = v/c$ is the speed in units of the speed of light. This concept had already been discovered by Rees (1967) before the first observations of strong variability (Dent 1965, Pauliny-Toth and Kellermann 1966, Sholomitskii 1965) and superluminal motion in radio jets (Cohen et al. 1977, Whitney et al. 1971) raised the questions for relativistic beaming. Finally the introduction of the twin relativistic jet model by Blandford and Rees (1974) formulated the observational consequences as:

$$\beta_{\text{app}} = \frac{\beta \sin \theta}{1 - \beta \cos \theta}, \quad (8)$$

which allows the observer to register superluminal motion in jets if the intrinsic jet speed, β , is close to the speed of light and the viewing angle, θ , is small (see Fig. 8). The maximum speed, $\beta_{\text{app,max}} = \sqrt{\gamma^2 - 1}$, occurs when $\cos \theta = \beta$ or $\sin \theta = \gamma^{-1}$. At this angle the Doppler factor is equal to the Lorentz factor. For the flux density one obtains:

$$S = S_0 \delta^{(3-\alpha)}, \quad (9)$$

where the spectral index α in the exponent corrects for the Doppler effect, which causes a frequency shift in the spectrum by the Doppler factor, δ . For a continuous jet the exponent changes to $(2 - \alpha)$ due to geometrical considerations (Scheuer and Readhead 1979).

Following equipartition arguments, Readhead (1994) found an even lower limit to the brightness temperature. The author states that if there is no large

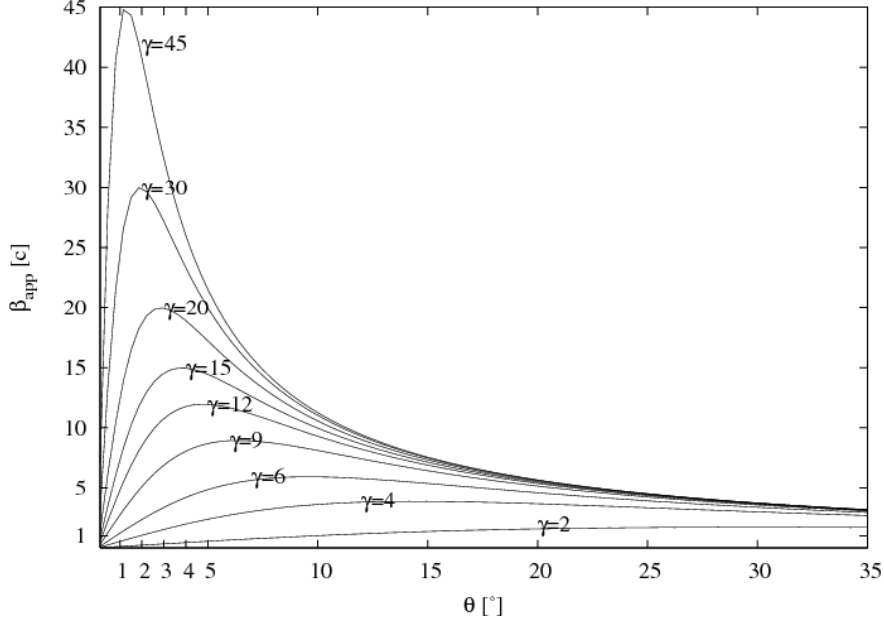


Figure 8: Illustration of the dependence of the apparent jet speed from the viewing angle and the intrinsic jet speed.

departure between the magnetic and the particle energy (equipartition), then the limiting brightness temperature is 5×10^{10} K to 10^{11} K.

Indeed jet speeds of up to 40 times the speed of light, corresponding to a minimum Lorentz factor of 40, have been measured (e.g. Jorstad et al. 2001b, Piner et al. 2006). Studies of the motion of AGN jet components is one of the main research fields of VLBI. In Figures 9 and 10 a time series of VLBA images taken at 7 mm and the corresponding identification of superluminal jet components in the jet of the radio galaxy 3C 120 are shown. Recently, detailed studies of individual sources are accompanied by large, statistically relevant surveys (Jorstad et al. 2001a, Kellermann et al. 2004, Lister 2005). So far, VLBI at radio frequencies is the only tool to spatially resolve the jets on parsec scales. Compact interferometers such as the VLA and MERLIN provide information on kilo-parsec scale jet motion (e.g. Laing and Bridle 2002) and in the optical the *Hubble* Space Telescope was used to measure motions in the optical jet of M 87 (Biretta et al. 1999). Although the most famous and usually also the brightest sources are those showing high superluminal motion with $\beta_{\text{app}} > 10 c$, most of the radio jets detected display much lower speeds of less than $3 c$ (Cohen et al. 2007, Kellermann et al. 2004, Lister 2005).

This is commonly interpreted as a result of the relativistic beaming model and reflects the fact that the sources are orientated at different angles to the line of sight. However, many of the low-velocity sources are high-power objects

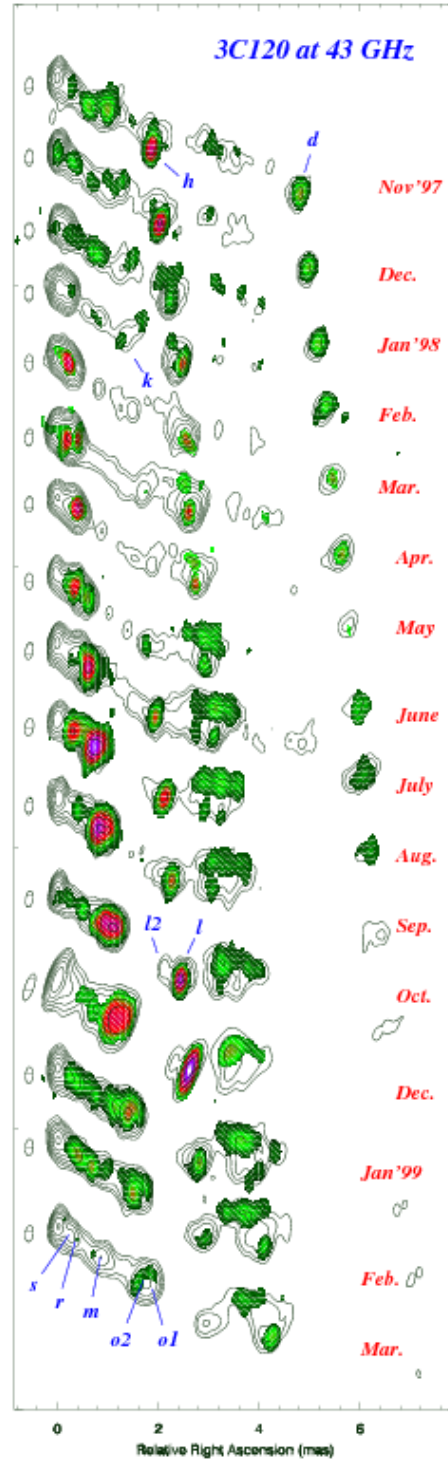


Figure 9: Time series of VLBA images of the jet of the radio galaxy 3C 120 showing many details of the structural evolution of the jet. Contours give the total intensity, colours (on a linear scale from green to white) show the polarized intensity, and bars (of unit length) indicate the direction of the magnetic polarization vector. Synthesized beams are plotted to the left of each image, with a typical size of 0.35×0.16 mas (courtesy Gómez et al. 2001).

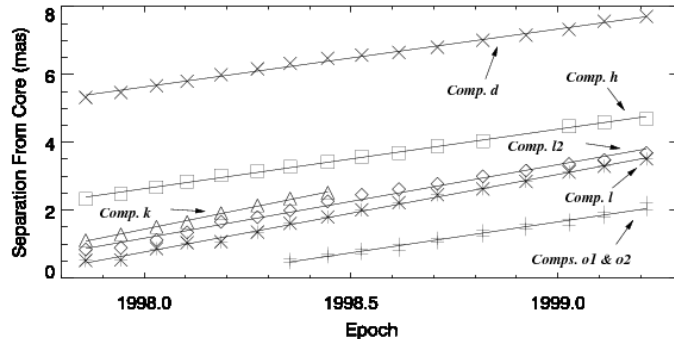


Figure 10: Projected angular distance from the core as a function of time for the superluminal components in the jet of 3C120. Those are the components which could be traced over the whole period shown in Fig. 9 (courtesy Gómez et al. 2001).

like quasars and BLLac objects. Their rapid variability and high brightness temperatures suggest that the bulk motion of the jet is highly relativistic. Some of them might have very small viewing angles corresponding to the region left of the peaks in Fig. 8, which reduces the apparent speed, but the probability that they are all oriented at very small angles to the line of sight is quite small (e.g. Cohen et al. 2007). It is more likely that the observed speed in those jets does not correspond to the maximum speed of the flow itself. Indeed there are a number of sources where components at different speeds are observed, something which cannot be explained by jet bending or variable Lorentz factors. In several other cases the speeds measured at higher spatial resolution are substantially higher than the measured speeds at lower resolution (e.g. Jorstad et al. 2001a, Kellermann et al. 2004).

For radio galaxies which generally show lower jet speeds increased evidence for structured jets is found. In this case the jet is expected to consist of a fast spine whose radio radiation is beamed away from our line of sight, surrounded by a slower sheath (e.g. Agudo et al. 2001, Cohen et al. 2007, Kellermann et al. 2004, Laing and Bridle 2002, Laing et al. 1999). Seyfert galaxies, which usually display motions of $< 0.5c$, are supposed to have initially weaker jets, and they often show signs of interaction with the surrounding medium (e.g. Ulvestad 2003, and references therein). Nevertheless, superluminal motion has been observed in some sources after a bright outburst (e.g. Brunthaler et al. 2000).

3.1.4 The radio-loud / radio-quiet divide

Radio-loud AGN are sources where the ratio of the 5 GHz radio flux density to the optical R -band flux density is of the order of 10 or larger. Sources with lower ratios are called radio quiet. Only about 10 % of the AGN population are radio-loud objects, nevertheless, most of the VLBI studies are dealing with

those sources. VLA and VLBI observations of radio-quiet sources revealed that their appearance is quite similar to radio-loud objects exhibiting cores, jets, and lobe-like structures, but just a bit weaker (e.g. Kellermann et al. 1994, Ulvestad et al. 2005). Also the spectral characteristics are similar, and variability studies comparing samples of radio-loud and radio-quiet objects revealed that the variability time scales are independent of radio luminosity or radio-to-optical flux density ratio. This all leads to the conclusion that the physics of radio emission in the inner regions of all quasars is essentially the same, involving a compact, partially opaque core together with a beamed jet (e.g. Barvainis et al. 2005). The formation of powerful jets might depend on a fine tuning of several parameters like the spin of the black hole, the type of accretion flow, and a favourable magnetic field geometry (e.g. Ballantyne 2007). Currently many authors seem to prefer the spin theory. Wilson and Colbert (1995) suggested that the coalescence of two super-massive black holes (SMBHs) after the merger of two massive galaxies might spin up the black hole so that it can produce a powerful jet. If not the coalescence of SMBHs, at least the merger history of a galaxy seems to play an important role for the radio-loudness (Capetti and Balmaverde 2006). Although they are harder to image radio-quiet quasars provide important information on the launching of jets and are crucial for the development of a unified scheme for active galaxies.

3.1.5 Intraday variability

Since the discovery of intraday variability (IDV, i.e. flux density and polarization variations on time scales of less than 2 days) about 20 years ago (Heeschen et al. 1987, Witzel et al. 1986), it has been shown that IDV is a common phenomenon among extra-galactic compact flat-spectrum radio sources. It is detected in a large fraction of this class of objects (e.g. Kedziora-Chudczer et al. 2001, Lovell et al. 2003, Quirrenbach et al. 1992). The occurrence of IDV appears to be correlated with the compactness of the VLBI source structure on milli-arcsecond scales: IDV is more common and more pronounced in objects dominated by a compact VLBI core than in sources that show a prominent VLBI jet (Quirrenbach et al. 1992; see also Lister et al. 2001). In parallel to the variability of the total flux density, variations in the linearly polarized flux density and the polarization angle have been observed in many sources (e.g. Kraus et al. 2003; 1999a;b, Qian and Zhang 2004, Quirrenbach et al. 1989). The common explanation for the IDV phenomenon at cm wavelengths is interstellar scattering (e.g. Rickett 2001, Rickett et al. 1995). The most convincing argument for interstellar scintillation comes from observations of time-delays between the IDV pattern from the same source arriving at two widely separated telescopes Dennett-Thorpe and de Bruyn (2002). Another frequently observed phenomenon is the annual modulation of the variability time scale. This is interpreted in terms of the change of the relative velocity between the scattering screen and the velocity of the Earth as it orbits the Sun (e.g. Bignall et al. 2003, Dennett-Thorpe and de Bruyn 2003, Gabányi et al. 2007, Rickett et al. 2001). However some effects remain that cannot be easily explained by

interstellar scintillation and that are probably caused by the relativistic jets. (e.g. Qian et al. 2002; 1996, Qian and Zhang 2004). For example the correlated intra-day variability between radio and optical wavelengths, which is observed in sources such as 0716+714 and 0954+658, suggests that at least part of the observed IDV has a source-intrinsic origin (e.g. Quirrenbach et al. 1991, Wagner et al. 1990; 1996). Also the recent detection of IDV at millimetre wavelengths in 0716+714 (Agudo et al. 2006, Kraus et al. 2003, Krichbaum et al. 2002b) is a problem for the interpretation of IDV by interstellar scintillation, because scintillation decreases with the square of the observing frequency.

Independent of the physical cause of IDV (source intrinsic, or induced by propagation effects), it is clear that IDV sources must contain one or more ultra-compact emission regions. Using scintillation models, typical source sizes of a few tens of micro-arcseconds have been derived (e.g. Bignall et al. 2003, Dennett-Thorpe and de Bruyn 2002, Rickett et al. 1995). In the case of source-intrinsic variability and when using arguments of light travel times, even smaller source sizes of a few micro-arcseconds are obtained. Then apparent brightness temperatures of up to 10^{18-19} K (in exceptional cases up to 10^{21} K) are inferred, far in excess of the inverse Compton limit of 10^{12} K. These high brightness temperatures can be reduced by relativistic beaming with high Doppler-factors (e.g. Kellermann 2002, Qian et al. 1996; 1991). It is currently unclear if Doppler-factors larger than 50 to 100 are possible in compact extragalactic radio sources (see Sect. 3.1.3 for more details on observed jet speeds). Space VLBI observations revealed that the variability in 0716+714 originates from the core, but the core itself remains unresolved and no structural changes were observed on short time scales (Bach et al. 2006a). However, future space VLBI missions or millimetre VLBI should be able to resolve the inner structures and shed more light on the very compact regions of IDV sources.

3.1.6 Polarization in AGN jets

In the commonly accepted picture where accretion onto a black hole powers the AGN, it is believed that the jet is driven outwards via magnetic forces. The poloidal magnetic field is wound up by the accretion disk or the ergosphere of the black hole and therewith accelerates and collimates the jet (e.g. Meier et al. 2001). Therefore important information about the physical properties of the jet are provided by the order and the geometry of the magnetic field. Since the emission process in the radio band is synchrotron radiation, the most direct way to investigate magnetic fields is to study the linear polarization of jets. The first studies of linear polarization using VLBI observations were already performed more than 20 years ago (Cotton et al. 1984). More recent studies dealing with larger samples of AGN have dramatically increased our knowledge about the linear polarization properties of the various types of AGN (e.g. Cawthorne et al. 1993, Gabuzda and Cawthorne 1996, Gabuzda et al. 2000, Jorstad et al. 2007, Lister and Homan 2005, Lister and Smith 2000, Marscher et al. 2002, Pollack et al. 2003). The degree of linear polarization of the VLBI core of a typical radio-loud AGN is usually below 5 %, because the core region is optically thick and

the maximum expected degree of linear polarization for such a region is 10 %. In the optically thin regime, where most of the emitted synchrotron photons can escape from the source without being absorbed, the maximum degree can reach 75 % (Burn 1966). Indeed the observed degree of linear polarization in the jet reaches up to 50 %, confirming its origin to be optically thin synchrotron emission (e.g. Lister and Homan 2005). Usually the linear polarization in the jet is enhanced at the position of bright jet components (see also Fig. 9) suggesting the existence of shocks that increase the order of the magnetic field (e.g. Lister and Smith 2000).

At the transition from optically thick to thin synchrotron emission the polarization angle is supposed to rotate by 90° . This was observed in a number of sources at lower frequencies (e.g. OJ287 Gabuzda and Gómez 2001). The difficulty here and for the measurement of the electric vector position angle (EVPA) in general is that the radio polarization angle can be affected by Faraday rotation (Faraday 1933). This is a rotation of the EVPA which occurs when a linearly polarised electromagnetic wave travels through a region with free electrons and a magnetic field with a non-zero component along the line of sight. The intrinsic polarization angle χ_0 is related to the observed polarization angle χ by

$$\chi = \chi_0 + \text{RM}\lambda^2 \quad (10)$$

where λ is the observed wavelength and RM is the rotation measure. The linear relationship to λ^2 is the characteristic signature of Faraday rotation. The rotation measure depends linearly on the electron density, n_e , the component of the magnetic field parallel to the line of sight, B_{\parallel} , and the path length, l , through the plasma. Using units of m^{-3} , Tesla, and parsec, the rotation measure can be expressed as

$$\text{RM} = 8120 \int n_e B_{\parallel} dl \quad (11)$$

The RM can be determined using simultaneous multi-frequency observations, which then allow the recovery of the intrinsic polarization orientation.

Zavala and Taylor (2003; 2004) have conducted an RM study of about 40 AGN. The authors found that the cores of quasars have typical RMs of approximately 500 rad m^{-2} to several 1000 rad m^{-2} within 10 pc of the core. Jet RMs are typically 500 rad m^{-2} or less. The cores and the jets of the seven BLLac objects have RMs comparable to those of quasar jets. Radio galaxies were usually found to have depolarized cores and exhibit RMs in their jets varying from a few hundred to $10\,000 \text{ rad m}^{-2}$. A gradient in the foreground Faraday screen is invoked to explain the observed depolarization properties of the sample. The Faraday screen is likely located close to the relativistic jet, although its exact nature remains unclear. The line-of-sight magnetic fields inferred from the observation range from 10 pT to 60 pT in jets and to 100 pT in quasar cores.

The cores of quasars show higher RMs than BLLac objects, but, conversely, show lower degrees of linear polarization (e.g. Lister and Homan 2005). A

possible explanation is that at least part of the missing linear polarization in quasars is removed by Faraday depolarization, where the propagation of emission through different patches of a turbulent plasma produces stochastic Faraday rotation, which leads to an overall reduction of the observed linearly polarized component. Also the absence of linear polarization in radio galaxies might be attributed to Faraday depolarization. Since radio galaxy jets are often observed in the plane of the sky the cores are seen through the dense environment surrounding the core region (Zavala and Taylor 2004).

When corrected for the rotation measure the EVPA can give an estimate for the orientation of the magnetic field in the jet. It turns out that BLLac objects tend to have EVPAs parallel to the jet direction, but for quasars the correlation is not that obvious (e.g. Cawthorne et al. 1993, Gabuzda et al. 2000, Pollack et al. 2003). For optically thin emission this means that the magnetic field is orientated transverse to the jet direction. Initially this was interpreted as evidence for transverse shocks which enhance the magnetic field component in this direction (e.g. Hughes et al. 1989). However, the effect can also be explained in terms of helical magnetic field structures, which are likely to be present in the inner jet (Lyutikov et al. 2005). Larger statistics and the correlation with properties from other wavelengths appear to be the methods that will help to disentangle the different effects (e.g. Jorstad et al. 2007, Lister and Homan 2005).

Another option to probe the particle population and magnetic field structure of the jets are studies of circular polarization (CP) on parsec scales. Early single dish observations showed that only marginal circular polarization ($< 0.1\%$) is present in AGN jets (Komesaroff et al. 1984, Weiler and de Pater 1983). Interferometric studies, however, detected CP in the cores of a number of sources (Homan et al. 2001, Homan and Wardle 1999; 2003; 2004, Wardle et al. 1998). A recent VLBI survey revealed circular polarization in the cores of 20 of a total of 133 observed AGN (Homan and Lister 2006). In two sources CP emission was detected also from separated jet components. Compared to the integrated values measured from single dish observations, VLBI images show higher levels of CP. About 15% of the cores have more than 0.3% of circular polarization and 0.3% to 0.5% were found in jet components. Circular polarization can be produced in two ways: as an intrinsic component of the emitted synchrotron radiation or via Faraday conversion of linear to circular polarization (Jones and O'dell 1977). The current statistics are not sufficient to determine the origin of CP, but when the intrinsic mechanism dominates, jets must be a predominantly electron-proton plasma and must contain a significant fraction of unidirectional ordered magnetic field. If the conversion mechanism dominates, circular polarization determines the low-energy end of the relativistic particle distribution (e.g. Wardle and Homan 2003), a key parameter in studying the bulk kinetic luminosity of AGN jets and their particle content (Celotti and Fabian 1993, Wardle et al. 1998). Since the composition of jets is one of the fundamental question in AGN research a lot of effort is currently put into the accurate determination of circular polarization in jets.

3.1.7 VLBI observations of circumnuclear tori

The previous sections have shown that AGN whose radio axes are close to the plane of the sky are the more difficult objects to study, because their jets are weaker, i.e. are less beamed, have low degrees of polarization and the central engine is highly obscured, which decreases the amount of additional information from optical and infrared wavelengths. However, in the radio, the obscuring material can be used to study the circumnuclear structures. There are mainly three observational methods: (i) molecular gas seen either masing (so far only water masers at 1.3 cm have been detected in AGN) or in absorption, (ii) atomic gas seen in absorption, and (iii) ionised gas revealed through free-free absorption.

1. Water masers are found predominantly in Seyfert 2 or LINER galaxies and are currently the only resolvable tracers of warm dense molecular gas in the inner parsec of AGN (e.g. Braatz et al. 2004; 1996, Greenhill et al. 2003b, Hagiwara et al. 2002, Henkel et al. 2005, Kondratko et al. 2006, Zhang et al. 2006). Because they are associated with nuclear activity, the most likely model for exciting the maser emission is X-ray irradiation of molecular gas by the central engine (e.g. Neufeld et al. 1994). In Mrk 348 the masers are located close to the receding jet, suggesting that the masers are likely to arise from the shock in front of the jet, rather than from continuum emission (Peck et al. 2003). About 60 AGN harbouring water masers are known up to date, but not all of them are bright enough to be observed with VLBI. The most relevant are NGC 4258 (Miyoshi et al. 1995), NGC 1386 (Braatz et al. 1997), NGC 4945 (Greenhill et al. 1997), NGC 1068 (Greenhill and Gwinn 1997), NGC 3079 (Kondratko et al. 2005, Middelberg et al. 2007), IC 2560 (Ishihara et al. 2001), and Circinus (Greenhill et al. 2003a). In these objects the maser emission appears to trace a nearly edge-on disk of molecular gas at distances of 0.1 pc to 1 pc from the supermassive black hole, which is supposed to be directly connected to the accretion disk.

The modelling of such maser sources can be used to determine parsec-scale accretion disk structures and to accurately estimate black hole masses (Greenhill et al. 2003a, Greenhill and Gwinn 1997, Herrnstein et al. 2005). Figure 11 shows the maser found in NGC 4258, which can be well fitted by a Keplerian rotation curve. When combined with the masers' proper motion or drifts in the line-of-sight velocities of spectral features (i.e., centripetal acceleration), those models can provide independent distance measurements to the galaxies and therewith even provide constraints for H_0 (Herrnstein et al. 1999). A recent VLBI study aims to measure the distance to the LINER NGC 4258 with an error of only 3% and, since the galaxy also contains Cepheid variable stars, will allow a direct comparison of the maser and Cepheid distances (Argon et al. 2007).

2. Evidence of a circumnuclear torus of atomic gas has been seen in Cygnus A (Conway 1999a), NGC 4151 (Mundell et al. 1995) and 1946+708 (Peck et al. 1999) and many young compact sources (e.g. Readhead et al. 1996,

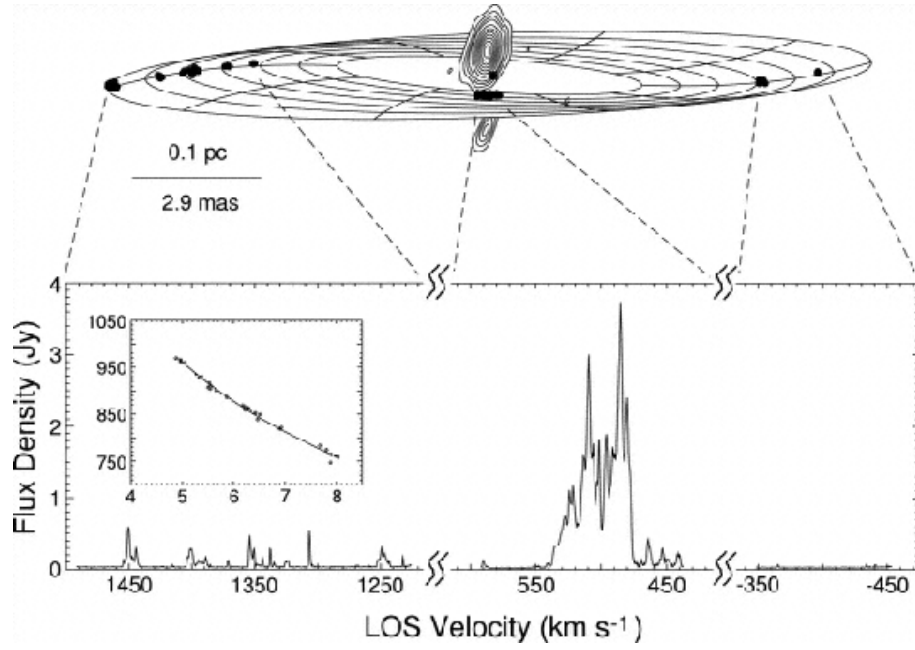


Figure 11: **Top:** Warped-disk model for the accretion disc in NGC 4258 with masers and continuum emission superposed. **Bottom:** Total power spectrum of the NGC 4258 maser, with best-fitting Keplerian rotation curve in the inset. Reprinted by permission from Nature (Herrnstein et al. 1999), copyright (1999) Macmillan Publishers Ltd.

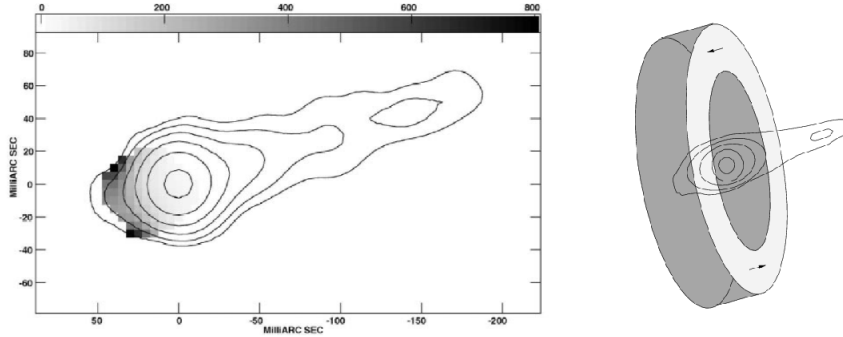


Figure 12: **Left:** Total intensity contours of the jet of Cygnus A with the HI opacity in greyscale (courtesy Conway 1999b). **Right:** The HI absorption is interpreted as the signature of a surrounding torus (courtesy Conway 1999a).

Vermeulen et al. 2003). In Cygnus A, HI absorption measurements with the VLBA indicate a torus with a radius of about 50 pc (Fig. 12). In NGC 4151, HI absorption measurements using MERLIN indicate a torus ~ 70 pc in radius and ~ 50 pc in height. One of the best examples of this type of torus is the Compact Symmetric Object (CSO) 1946+708. The HI absorption is found in front of all of the ~ 100 pc of its continuum emission, and the line widths, velocities and HI optical depth distribution are consistent with the scenario of a thick torus, consisting predominantly of atomic gas (Peck and Taylor 2001, Peck et al. 1999).

Because radio galaxies often have weak cores and jets, studies of circum-nuclear tori can only be carried out for sources with compact jets. One of the less powerful cases is the galaxy NGC 4261, where VLBI observations of HI absorption revealed the existence of a thin disk seen in projection against the counter-jet (van Langevelde et al. 2000). This shows that there are differences in the nuclear torus/disk system, which are important parameters for our understanding of AGN. Therefore this is one of the science drivers for more sensitive instruments like the SKA.

3. Parsec-scale radio counter-jets are important for studying the intrinsic symmetry of the jet-formation process, and are probes of the structure of ionised gas in the central parsec of AGN. The latter case becomes noticeable as free-free absorption in front of the counter-jet. If geometrically thin, the disk will cover only the inner part of the counter-jet but not the approaching jet. If geometrically thick, the core and perhaps the base of the approaching jet may also be absorbed. Multi-frequency observations can detect the highly inverted spectrum created by free-free absorption. This has been found in a number of cases. For example in 3C 84 (Walker et al. 2000) and in the aforementioned case of NGC 4261 (Jones et al. 2001) where HI absorption as well as free-free absorption has been found.

In the FR II radio galaxy Cygnus A multi-frequency VLBI observations revealed a deep gap between the core and the counter-jet at lower frequencies, which changes to an inverted spectrum at high frequencies (Bach et al. 2005, Krichbaum et al. 1998a). Since HI absorption was found at the base of the counter-jet (Fig. 12, Conway 1999a) the gap most likely indicates free-free absorption.

3.1.8 The Galactic Centre

The compact radio source at the centre of the Milky Way was found by Balick and Brown (1974) and was named Sagittarius A* (Sgr A*, Brown 1982) to distinguish it from the larger-scale galactic region Sgr A. A comprehensive review on the galactic centre and Sgr A* was recently given by Melia and Falcke (2001). The association with a supermassive black hole had already been suggested before its discovery by Lynden-Bell and Rees (1971), and was subsequently supported by a number of observations, e.g. by proper motion measurements of stars in the vicinity of the galactic centre (Eckart and Genzel 1996; 1997, Ghez et al. 1998) and from size estimates from VLBI observations (e.g. Bower et al. 2004; 2006, Doeleman et al. 2001, Krichbaum et al. 1998b, Rogers et al. 1994, Shen et al. 2005). Because of the proximity of Sgr A* high-resolution VLBI images provide a very high linear resolution. Adopting a distance of 8 kpc and a mass of $4 \times 10^6 M_\odot$ (Eisenhauer et al. 2003, Ghez et al. 2005), 0.1 mas correspond to $10 R_S$ (Schwarzschild radii, $1 R_S = 1.2 \times 10^{12}$ cm). VLBI observations of Sgr A* can therefore help to distinguish between the many different models for the emission, accretion, and outflow physics of the source, as well as provide an important test of strong-field gravity (e.g. Falcke et al. 2000).

The main problem in determining the size of Sgr A* is that its true structure is affected by scattering in the interstellar medium, leading to a λ^2 dependence of its diameter as a function of the observed wavelength. Up to 43 GHz this results in an elliptical profile orientated at an angle of $\sim 80^\circ$, the axes of which follow $\theta_{\min} = 0.76 \text{ mas } (\lambda/\text{cm})^2$ and $\theta_{\max} = 1.42 \text{ mas } (\lambda/\text{cm})^2$ (Lo et al. 1998). At 43 GHz and higher frequencies there is growing evidence that the intrinsic source size becomes visible (e.g. Doeleman et al. 2001, Krichbaum et al. 2006; 1998b, Rogers et al. 1994).

More recent efforts using the technique of closure amplitudes (e.g. Doeleman et al. 2001), which reduces sensitivity but removes uncertainties due to calibration errors, have resulted in a more robust detection of the intrinsic source size of Sgr A*. Bower et al. (2004; 2006) and Shen et al. (2005) determined diameters of $\sim 10 R_S$ to $\sim 13 R_S$ at 86 GHz, which is consistent with an estimate of $11 \pm 6 R_S$ from earlier VLBI measurements at 215 GHz (Krichbaum et al. 2006; 1998b). The peak brightness temperature was estimated to be 10^{10} K at 86 GHz, which mainly excludes advection-dominated accretion flows (Narayan et al. 1998) and Bondi-Hoyle accretion models (Melia 1994). Because of the limited sensitivity in the minor axis size of the scattering ellipse the current measurements are not able to distinguish between jet models (Falcke et al. 1993), generic radiatively inefficient accretion flows (Quataert and Gruzinov 2000), and hybrids of

these models (Yuan et al. 2002). Future arrays including telescopes such as the Large Mexican Telescope (LMT), APEX, and ALMA, which provide a better uv-coverage and increased performance at frequencies above 90 GHz will put further constraints on the minor axis and might be able to image the shadow of the black hole itself (e.g. Falcke et al. 2000).

3.2 Stars

Stars are not the primary targets for VLBI observations, because their brightness temperatures (10^3 K to 10^4 K) are much less than those required for VLBI detections (10^6 K). Nevertheless, observations of phenomena associated with stars can be made in a few cases, which will be reviewed in this section.

3.2.1 Circumstellar disks and envelopes

Mira-type variable stars are frequent targets of VLBI observations. Mira stars have a few solar masses and have reached the end of their lives where the outer envelopes become very extended. The envelope becomes cool enough for molecules to form, and hence maser emission can be observed in these objects.

One of the best-studied Mira stars is TX Cam, the SiO $v = 1$, $J = 1 - 0$ maser emission of which has been observed by Diamond and Kemball (2003) over a period of almost two years, corresponding to a full pulsation period. When combined into a movie¹⁰, the 44 images, showing the ring-like maser emission of TX Cam in biweekly intervals, are a fascinating documentary of the evolution of a star. It was found that the shell from which the emission arises is mostly non-symmetric, and that gas on outward trajectories shows evidence for gravitational deceleration. Further observations by Yi et al. (2005) indicated that the red- and blueshifted masers were evenly distributed around the star, indicating that it is not rotating.

Polarimetric observations of SiO masers in Mira, U Ori, and R Aqr reported by Cotton et al. (2006) indicate that masing material is being dragged by magnetic fields in the star. Furthermore, the authors report possible rotation for only Mira, though this finding could be affected by Mira's binary companion.

The envelopes of evolved stars can be observed also using H₂O masers. In particular, Vlemmings et al. (2002) and Vlemmings et al. (2005) report measurements of circular polarization of H₂O masers in evolved stars to determine stellar magnetic fields via the Zeeman effect. They report magnetic field strengths of several hundred milligauss to one gauss, and have modelled the stellar magnetic fields as dipoles (Figure 13).

OH masers trace gas with much lower densities than SiO and H₂O masers. Claussen et al. (1999) and Hoffman et al. (2005) report VLBI detections of OH masers in, e.g., W28, which Hoffman et al. (2005) ascribe to the interface between the supernova remnant and a molecular cloud. From Zeeman splitting they infer magnetic fields of the order of one milligauss in W28.

At the other end of stellar life cycles, maser observations can yield information about star formation. Magnetic fields are thought to play important roles in the formation of massive stars, and have consequently been observed via polarimetric VLBI observations of H₂O masers, e.g., in Cepheus A (Vlemmings et al. 2006b), W51 M (Leppänen et al. 1998), and Orion KL and W3 IRS 5 (Imai et al. 2003).

¹⁰<http://www.journals.uchicago.edu/ApJ/journal/issues/ApJ/v599n2/58473/video2.mpg>, or <http://www.nrao.edu/pr/1999/txcam/txcam.a-ak.gif>

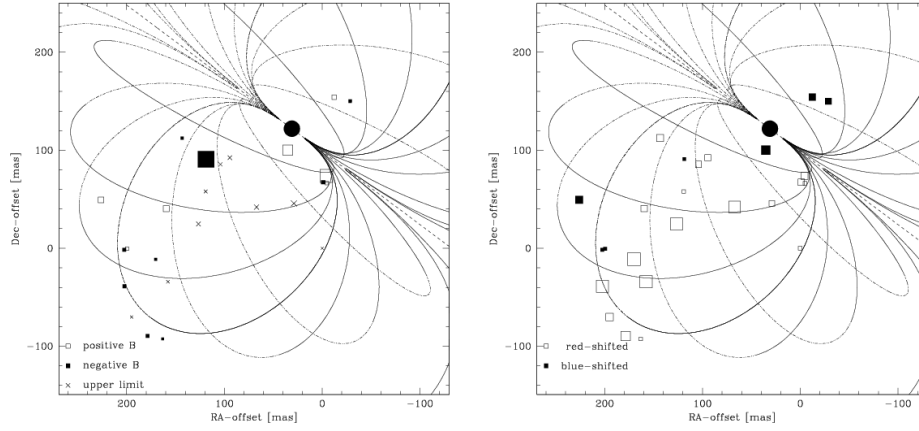


Figure 13: A sketch of the dipole magnetic field in VX Sgr as derived from H_2O maser observations by Vlemmings et al. (2005). The left panel shows the magnetic field orientation (positive or negative) and the symbol sizes scale with the magnetic field strength. The right panel shows the velocity distribution of the maser features, showing red- and blueshifted components. Symbol sizes indicate the velocity difference. Reproduced with kind permission of the author.

3.2.2 Stellar jets

It has been postulated that magnetic fields confine jets of evolved stars. This could explain the asymmetric shapes of planetary nebulae, the remnants of stars. Vlemmings et al. (2006a) present evidence for magnetic confinement of the jet of W43A, using polarimetric VLBI observations of its H_2O maser emission.

3.2.3 Supernovae

Some supernovae have brightness temperatures high enough for their continuum emission to be detected with VLBI arrays. Almost all of these are core-collapse supernovae of Types II and Ib/c. They give astronomers the unique opportunity to observe the geometric evolution of supernovae, and some remarkable observations have been carried out in the last few years.

The most prominent supernova that has been studied with VLBI probably is SN 1993J in the nearby galaxy M81. Marcaide et al. (1993) discovered early on that the supernova could be detected on intercontinental baselines and began a monitoring campaign. Marcaide et al. (1995a) found that the supernova had a shell-like structure and Marcaide et al. (1995b) found the shell to expand symmetrically, indicating that the shell was expanding into a homogeneous medium. Hints of deceleration were reported in 1997 by Marcaide et al. (1997) and were confirmed by Bartel et al. (2000), who had monitored SN1993J at regular intervals with the VLBA since the explosion. Bartel et al. (2000) also found that the deceleration of the expansion could not be explained with the

“standard” model by Chevalier (1982). They inferred from the progress of deceleration that SN1993J had left the phase of free expansion and had entered a phase of adiabatic expansion, which is dominated by the swept-up circumstellar material.

VLBI observations have recently also been used to search for supernovae. Though not all attempts have been fruitful (Ulvestad et al. 2007), sometimes interesting serendipitous discoveries are made (Neff et al. 2004). In star-forming galaxies, the densities of massive stars, and consequently the rate of supernovae, is so high that explosions can be observed on time scales of years. Lonsdale et al. (2006) have observed the prototypical ultra-luminous infrared galaxy Arp 220 with a very sensitive global VLBI array, and discovered 49 point-like sources which they identified as predominantly young supernovae. Comparing their observations to images made 12 months earlier they were able to identify four supernovae which had exploded in the time between the observations. Comparing their findings to the luminosities of supernovae in the nearby star-forming galaxy M 82, they confirm that the star formation in Arp 220 is like that in M 82 but scaled up by a factor of a few tens.

3.2.4 X-ray binaries

X-ray binaries (XRBs) are thought to consist of a compact star (a neutron star or a black hole), and a donor star from which matter is transferred onto the compact companion. Some XRBs exhibit radio emission and, because the accretion and emission mechanisms are thought to be similar to those in quasars, XRBs are sometimes called microquasars.

The properties of XRBs, when compared to quasars, scale very roughly with luminosity, and this is also true for the time scales on which they evolve. XRBs are variable on time scales of days, or even hours. Fomalont et al. (2001) demonstrated this very clearly on Sco X-1, observing the object continuously for more than two days, using three VLBI arrays¹¹. Their images show a two-sided structure with radio-emitting components moving away from a central radio component as the observation progressed. The components ejected from the nucleus travelled at approximately half the speed of light. VLBI observations of the microquasar GRS 1915+105 by Dhawan et al. (2000) had already found speeds in excess of the speed of light, which arose from a projection effect and is common in observations of AGN jets. Similarly, Miller-Jones et al. (2004) find that Cyg X-1 displays a two-sided jet morphology with mildly relativistic speeds. Another instructive movie, made from daily VLBA 1.5 GHz snapshots over the course of six weeks, shows the microquasar SS 433¹² (Mioduszewski et al. 2004). The observations showed that the jet ejecta brighten at specific distances from the nucleus, but only at certain times in the 164-day precession period of the accretion disk, indicating a non-symmetric obstacle with which the jet collides.

¹¹see also <http://www.nrao.edu/pr/2001/scox1/scox100.htm>

¹²<http://www.nrao.edu/pr/2004/ss433>

VLBI observations have recently helped to determine the nature of the XRB LSI+61303. It had been debated whether the emission is microquasar-like or due to a pulsar wind nebula (an illustration of these competing models can be found in Mirabel 2006). The morphology of the mas-scale radio emission, monitored over one orbital period of the binary by Dhawan and Rupen (2006), indicates that the radio emission is due to a pulsar wind nebula; the emission has a cometary appearance and points away from the high-mass companion throughout the orbit of the neutron star.

3.3 Results from astrometric observations

VLBI observations not only provide extremely high resolution but can also yield very accurate measurements of the positions of radio sources. In this section we describe recent results from VLBI observations where the positional accuracy was essential.

3.3.1 Reference frames

Assigning a coordinate to a celestial object is not trivial. The earth rotates, precesses and nutates, its surface changes via tectonic plate motions, its angular velocity decelerates as a result of tidal friction due to the moon’s orbit, and the solar system rotates around the Galactic centre at a speed of 220 km s^{-1} . Furthermore, planets, stars and other celestial bodies have proper motions and change their appearances and shapes, even on time scales of years or less. Hence it is important to have a coordinate system (a reference system) that is tied to celestial phenomena that change as little as possible (a reference frame, which is an implementation of the reference system), and which can be defined as accurately as possible. The current reference frame adopted by the International Astronomical Union is the International Celestial Reference Frame, or ICRF (Ma et al. 1998), which is based on VLBI observations of point-like, strong, distant quasars. This reference frame satisfies the two aforementioned requirements: quasars are very distant and are not connected with one another in any way, hence no rotation is expected, and their positions can be observed with very high accuracy. Previous reference frames such as the “Fifth Fundamental Catalogue” (Fricke et al. 1988) had been established by observations of several thousand stars and had accuracies of the order of tens of mas. Stars, however, have detectable proper motions and are gravitationally bound in the Milky Way, and the accuracy of their position measurements are much lower than those of typical VLBI observations. The 212 “defining” sources in the ICRF have typical position errors of 0.4 mas, and the orientation of the axis defined from this set of sources has an accuracy of 0.02 mas. A complication with using VLBI observations of quasars though is that radio jets structures are subject to changes, which needs to be taken into account for these measurements. A good review about reference systems, reference frames and the implementation of the ICRF can be found in Feissel and Mignard (1998). Another application of astrometric observations is to calibrate Global Positioning System (GPS) measurements. Some VLBI stations are outfitted with GPS receivers, the positions of which are determined using astrometric observations. The same GPS receivers are then used to determine errors in the orbits of GPS satellites.

Lestrade et al. (1999) have carried out VLBI observations of 11 radio-emitting stars to tie the Hipparcos reference frame to the ICRF. In addition to the Hipparcos link, these observations also had astrophysical implications for the observed stars. For example, they found that the binary UX Ari exhibits significant acceleration, which could be caused by a yet unknown companion.

3.3.2 Distances and proper motions of stars and masers in the Milky Way

Stars can be observed only if they emit non-thermal radiation, which is typically the case for T Tauri stars. Torres et al. (2007) report on VLBI observations of Hubble 4 and HDE 283572, two T Tauri stars in the Taurus association. They infer distances of (132.8 ± 0.5) pc and (128.5 ± 0.6) pc, respectively, which is an order of magnitude more accurate than other distance measurements. In a companion paper, Loinard et al. (2007) report a similar measurement for T Tauri itself.

Sandstrom et al. (2007) present a similar measurement for the star GMR A in the Orion Nebula Cluster. They find a distance of (389^{+24}_{-21}) pc, in disagreement with the hitherto canonical value of (480 ± 80) pc reported by Genzel et al. (1981). Placing the Orion cluster at a distance 20 % smaller than previously thought implies that the luminosities of stars within it are lower by a factor of 1.5 – and that the stars are almost twice as old, since age scales as luminosity to the $-3/2$ power.

As was mentioned in the overview of the world’s VLBI arrays, Japan has built a four-station network specifically for precise astrometry of Galactic masers, and first results are beginning to be published: Hirota et al. (2007b) report VLBI observations of the water maser emission from Orion KL over two years, from which they derive a trigonometric distance of (437 ± 19) pc. This measurement is difficult to reconcile with the result reported by Sandstrom et al. (2007) – which is the correct value time will show. In two other papers, Hirota et al. (2007a) report a similar measurement of the distance to the young stellar object SVS 13 in NGC 1333, and Honma et al. (2007) have measured the distance to the star-forming region Sharpless 269, finding a value of $(5.28^{+0.24}_{-0.22})$ kpc (or a parallax of $189 \pm 8 \mu\text{as}$), which they claim is the smallest parallax ever measured (and indeed *is* more precise than the parallax of Sco X-1 measured by Bradshaw et al. 1999, who obtained $(360 \pm 40) \mu\text{as}$ and had once claimed the record).

Focussing on distances to evolved stars, Vlemmings and van Langevelde (2007) have observed the OH maser transition at 1.6 GHz in the envelopes of S CrB, RR Aql, and U Her. Their measurements have accuracies of 4 % to 34 %, which is a vast improvement over older Hipparcos measurements, with errors of 50 % to 100 %.

3.3.3 Distances and proper motions of pulsars

The only model-independent method to determine the distance to a celestial object is the trigonometric parallax. From optical observations, parallaxes can be obtained only for close objects. Remember that the positional accuracy of optical observations is limited to about $0.1''$ and therefore parallaxes can be measured for objects within only 10 pc. VLBI observations, however, can yield positions as good as 0.1 mas and so one can measure parallaxes of objects at a distance of up to 10 kpc. Pulsars are among those few objects that have brightness temperatures high enough for VLBI observations and it is known that they

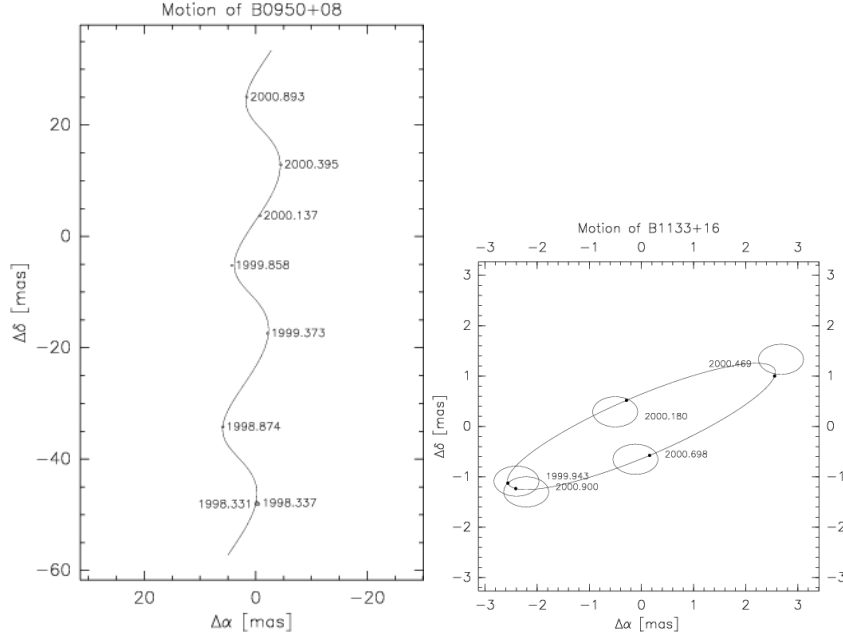


Figure 14: Illustration of the combination of proper motion and parallax motion of pulsars observed with VLBI (Briskin et al. 2002). The left panel shows the observed locations of the pulsar B0950+08 over the course of 2.5 yr. The track is a combination of the pulsar’s proper motion and the earth’s rotation around the sun. To indicate the significance of such parallax measurements, the modelled proper motion of the pulsar B1133+18 has been subtracted in the right panel, clearly showing the annual parallax (the small ellipses indicate the position errors). Reproduced with kind permission of the author.

are point sources (this is even true for VLBI observations). Parallax measurements can therefore yield distances to pulsars in large portions of the Milky Way and help to calibrate the distance scale derived from the pulse dispersion measurements obtained from single-dish observations.

Only a handful of pulsar parallaxes had been measured until 2000 (for a list and references see Table 1 in Briskin et al. 2002). This has changed in the last few years, and many more measurements are now becoming available (e.g., Briskin et al. 2002, Dodson et al. 2003, Chatterjee et al. 2005, and Helfand et al. 2007). These observations not only added to the number of trigonometric parallaxes, but also yielded pulsar proper motions (transverse to the line of sight). Proper motion measurements allow one to determine the likely birth places, as done by Ng et al. (2007), help to constrain velocities derived from pulsar timing, or, in some cases, are the only available velocity measurements when pulsar timing is not possible (e.g., Dodson et al. 2003).

3.3.4 Proper motions of galaxies in the Local Group

Measurements of the proper motions in the Local Group certainly is not a widely spread application of VLBI observations, but it illustrates the potential of high-precision position measurements.

Brunthaler et al. (2005) used the VLBA to monitor water masers in M33 over more than 4 yr. They were able to detect proper motion of $36 \mu\text{as yr}^{-1}$ in right ascension and $13 \mu\text{as yr}^{-1}$ in declination. Comparing these measurements to rotation models of M33 based on measurements of neutral hydrogen, they were able to infer a geometric distance to M33 of $(730 \pm 168) \text{ kpc}$. Together with similar measurements in the nearby galaxy IC 10 (Brunthaler et al. 2007), a picture of the dynamics in the Local Group begins to emerge (Fig. 15 and Loeb et al. 2005).

3.3.5 Gravitational lenses

Gravitational lenses in which the emission of a distant quasar is deflected by a foreground galaxy, producing multiple images extended over a few arcseconds, are obvious VLBI targets. High-resolution observations yield accurate separation measurements and can confirm that images belong to a lens because they have the same spectral indices, surface brightness, or degree of polarization. If the lensed object has sub-structure such as jets, then it becomes possible to investigate sub-structures in the lens galaxy.

For example, Bradač et al. (2002) have observed the lens system B1422+231 and are able to produce a reasonable model for the lens only when substructure is included (that is, they were unable to model the lens with a simple ellipsoid). Substructure in the lens can also be inferred from asymmetries in the lensed images, as has been tentatively found in B1152+199 by Rusin et al. (2002). Biggs and Browne (2002) report VLBI observations of B0128+437, and they speculate that the lens could have a halo of intermediate-mass black holes (“milli-lensing”). Finding substructure in the haloes of lensing galaxies may yield clues about large-scale structure formation, driven by a lack of halo dwarf galaxies in the Local Group.

Koopmans et al. (2002) and Porcas et al. (2002) present VLBI observations of MG 2016+112, in which one image of the background source is extremely stretched. This is interpreted as the radio jet of the lensed quasar crossing the caustic of the lens, leading to extreme magnification. Koopmans et al. (2002) speculate that with such high magnification one might be able to observe hyperluminal motion of the order of $(10^2 \text{ to } 10^3) c$.

Gravitational lenses offer the exciting opportunity to obtain a value for H_0 , using relatively simple astrophysics (Refsdal 1964). However, to constrain H_0 requires one to use a model of the mass distribution in the lensing object, which is mostly difficult to obtain (see Schechter 2005 for a review of the associated difficulties). Nevertheless, York et al. (2005) present an estimate from observations of CLASS B0218+357 with radio interferometers on all scales and Hubble Space Telescope observations. They derive values of $(70 \pm 5) \text{ km s}^{-1} \text{ Mpc}^{-1}$ and

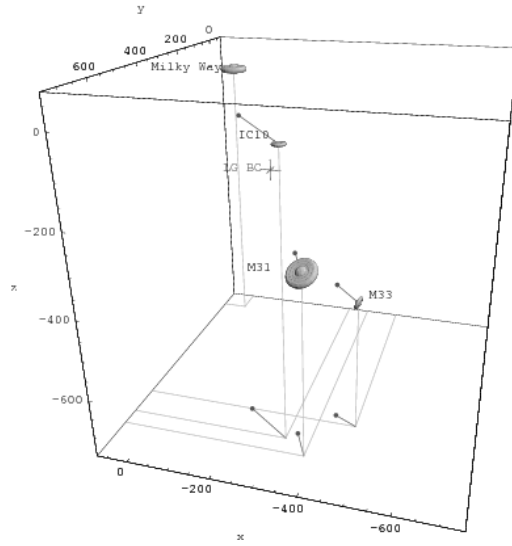
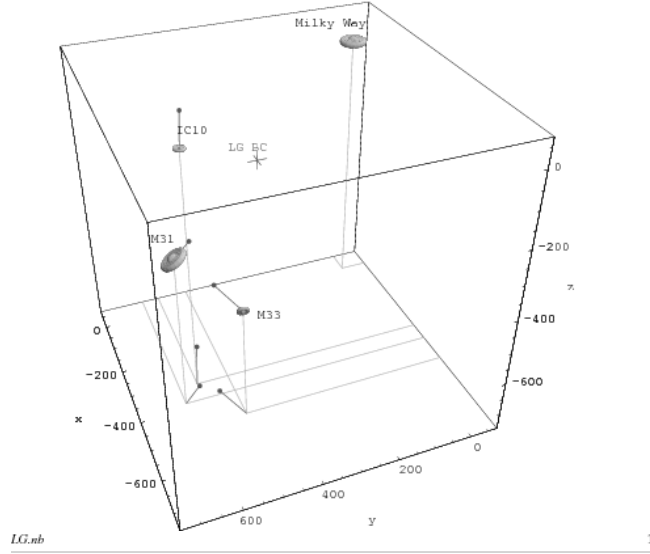


Figure 15: The relative positions and velocities of galaxies in the Local Group as determined by Brunthaler et al. (2005). Reproduced with kind permission of the author.

$(61 \pm 7) \text{ km s}^{-1} \text{ Mpc}^{-1}$, depending on the treatment of the lensing galaxy.

We refer the reader to the reviews by Porcas (2004) and Biggs (2005) for more information about gravitational lenses and VLBI.

3.3.6 Measurement of the speed of gravity waves

General relativity predicts that light is deflected by matter, something which had been measured for the first time by Dyson et al. (1920), who were able to measure the deflection of a star near the sun during a solar eclipse. In 2002 Fomalont and Kopeikin (2003) have carried out an experiment to measure the deflection of the light of a quasar as Jupiter passed within $3.7'$, by monitoring the position of the quasar relative to two other quasars over eight days with an accuracy of less than $10 \mu\text{as}$. They were able not only to measure the effects of Jupiter's mass, but also those of Jupiter's velocity. The observed deflection matched the predictions from General Relativity, but a controversy emerged over whether the result depends on the speed of gravity waves, c_g , or the speed of light, c (Carlip 2004; 2005, Kopeikin 2005).

3.3.7 Spacecraft tracking

In 2005, a global VLBI array has been used to carry out a unique experiment. The Cassini spacecraft, exploring Saturn, launched a probe called Huygens onto Saturn's moon Titan. The goal was to measure parameters like temperature, pressure, and wind speeds as the probe would descent towards Titan's surface, hanging from a parachute. The winds were to be measured using Doppler measurements in the radio signal from Huygens to Cassini (the so called Doppler Wind Experiment, DWE), the only communication link from the Titan probe. Unfortunately, one of Cassini's receivers failed, resulting in the potential loss of the DWE data transmitted by Huygens. The solution of this problem was to measure Huygens' path and horizontal velocity in the atmosphere by tracking, or rather eavesdropping on, its uplink to Cassini with a global VLBI array. The Huygens radio link was designed to operate between Huygens and Cassini, some 100 000 km apart, not between Huygens and Earth at 1.2 billion kilometres. Thus, the Huygens signal at Earth was very weak (measured in tens to hundreds of photons per telescope per second). In addition, most of the Huygens descent took place while Saturn was best visible from the Pacific ocean – an area sparsely populated by radio telescopes. The experiment succeeded nevertheless, resulting in extraordinarily accurate data on the descent trajectory (with 1 km accuracy) and horizontal velocity. The observers were even able to detect the swinging of Huygens below its parachute, with an amplitude of 0.6 m (Gurvits, priv. comm.).

3.3.8 Motion of the sun around the Galactic centre

The nature of the compact radio source in the Galactic Centre, Sgr A*, has been the target of many VLBI observations (see Section 3.1.8). Evidence from astrometric observations of the central mass in Sgr A* was presented by Reid et al.

(1999). They monitored the position of Sgr A* over two years with a VLBI array, and found that its apparent motion in the Galactic plane is $(5.90 \pm 0.4) \text{ mas yr}^{-1}$. This motion of course is caused by the sun's orbit around the Galactic centre. When the sun's orbit (known from other observations) was taken into account, the proper motion of Sgr A* is less than 20 km s^{-1} . This means that Sgr A* is extremely close to the dynamic centre of the galaxy. Were the radio emission from Sgr A* emitted by an exotic form of stellar cluster, then much higher velocities would be expected. Taking into account the mass of the stars orbiting Sgr A*, which is of the order of $10 M_{\odot}$, and their high velocities of a few hundred kilometres per second, the negligible proper motion of Sgr A* implies that it must have a mass of at least $1000 M_{\odot}$. All evidence is consistent with Sgr A* being a black hole.

4 Conclusions

In the general astronomical community VLBI observations are often considered to be rather exotic, because the technique is regarded as complicated and its range of application limited to AGN. We acknowledge that VLBI observations, and in particular the data calibration, can be a challenge, but we have shown here that the technique is applicable to a surprisingly broad variety of astrophysical objects and problems. We wish to highlight a few key contributions.

The structure and evolution of plasma jets ejected from compact objects such as black holes and neutron stars would not have been possible without VLBI. In particular multi-epoch observations have revealed the evolution of plasma jets and yielded constraints on their structure, physics, and environment.

In the Milky Way a key contribution of VLBI observations are proper motions and parallaxes for stars, masers, and pulsars. These observations are a reference for other measurements of distances and so are fundamental for the interpretation of other observations, and to derive a consistent picture of the Milky Way's structure.

A more general application is the use of VLBI to implement a reference frame, which is used throughout observational astronomy. These observations not only tell us where objects are, but they also tell us how fast the earth rotates, and hence how to set our clocks, and how observations at different wavelengths fit together.

Recent advances in computer technology have had profound impact on VLBI observations, and will do so in the near future. Directly-linked antennas will become the standard mode of operation at many VLBI facilities, and software correlators will allow observers to image wider fields of view, and to use more bandwidth to increase sensitivity and (u, v) coverage. The most relevant improvement however will be the SKA: it will be sensitive enough for observations of thermal sources. At mas-scale resolution, the SKA will image many astronomical objects which are inaccessible today.

References

- Agudo, I., Bach, U., Krichbaum, T. P., et al. 2007, “Superluminal non-ballistic jet swing in the quasar NRAO 150 revealed by mm-VLBI”. *A&A*Letters, in press, (astro-ph/0710.5435)
- Agudo, I., Gómez, J.-L., Martí, J.-M., et al. 2001, “Jet Stability and the Generation of Superluminal and Stationary Components”. *ApJ*, 549, L183
- Agudo, I., Krichbaum, T. P., Ungerechts, H., et al. 2006, “Testing the inverse-Compton catastrophe scenario in the intra-day variable blazar S5 0716+71. II. A search for intra-day variability at millimetre wavelengths with the IRAM 30m telescope”. *A&A*, 456, 117
- Antonucci, R. 1993, “Unified models for active galactic nuclei and quasars”. *ARA&A*, 31, 473
- Antonucci, R. R. J. and Miller, J. S. 1985, “Spectropolarimetry and the nature of NGC 1068”. *ApJ*, 297, 621
- Argon, A. L., Greenhill, L. J., Reid, M. J., et al. 2007, “Toward a New Geometric Distance to the Active Galaxy NGC 4258. I. VLBI Monitoring of Water Maser Emission”. *ApJ*, 659, 1040
- Baade, W. and Minkowski, R. 1954, “Identification of the Radio Sources in Cassiopeia, Cygnus A, and Puppis A.” *ApJ*, 119, 206
- Bach, U., Kadler, M., Krichbaum, T. P., et al., “Multi-Frequency and Multi-Epoch VLBI Study of Cygnus A”, in: J. D. Romney and M. J. Reid (eds.), *ASP Conf. Ser. 340: Future Directions in High Resolution Astronomy*, p. 30 (ASP, San Francisco, CA, 2005)
- Bach, U., Krichbaum, T. P., Kraus, A., et al. 2006a, “Space-VLBI polarimetry of the BL Lacertae object S5 0716+714: rapid polarization variability in the VLBI core”. *A&A*, 452, 83
- Bach, U., Villata, M., Raiteri, C. M., et al. 2006b, “Structure and flux variability in the VLBI jet of BL Lacertae during the WEBT campaigns (1995-2004)”. *A&A*, 456, 105
- Balick, B. and Brown, R. L. 1974, “Intense sub-arcsecond structure in the galactic center”. *ApJ*, 194, 265
- Ballantyne, D. 2007, “The Accretion Geometry in Radio-Loud Active Galaxies”. *Modern Physics Letters A*, 22, 2397
- Bartel, N., Bietenholz, M. F., Rupen, M. P., et al. 2000, “The Changing Morphology and Increasing Deceleration of Supernova 1993J in M81”. *Science*, 287, 112

- Barvainis, R., Lehar, J., Birkinshaw, M., et al. 2005, “Radio Variability of Radio-quiet and Radio-loud Quasars”. *ApJ*, 618, 108
- Beasley, A. J., Gordon, D., Peck, A. B., et al. 2002, “The VLBA Calibrator Survey-VCS1”. *ApJS*, 141, 13
- Begelman, M. C., Blandford, R. D., and Rees, M. J. 1984, “Theory of extragalactic radio sources”. *Reviews of Modern Physics*, 56, 255
- Biggs, A., “Gravitational Lenses and VLBI”, in: J. Romney and M. Reid (eds.), *Future Directions in High Resolution Astronomy*, vol. 340 of *Astronomical Society of the Pacific Conference Series*, p. 433 (2005)
- Biggs, A. D. and Browne, I. W. A., “Multi-frequency VLBI observations of the lens system B0128+437”, in: E. Ros, R. W. Porcas, A. P. Lobanov, and J. A. Zensus (eds.), *Proceedings of the 6th EVN Symposium*, p. 193 (2002)
- Bignall, H. E., Jauncey, D. L., Lovell, J. E. J., et al. 2003, “Rapid Variability and Annual Cycles in the Characteristic Timescale of the Scintillating Source PKS 1257-326”. *ApJ*, 585, 653
- Biretta, J. A., Moore, R. L., and Cohen, M. H. 1986, “The evolution of the compact radio source in 3C 345. I - VLBI observations”. *ApJ*, 308, 93
- Biretta, J. A., Sparks, W. B., and Macchetto, F. 1999, “Hubble Space Telescope Observations of Superluminal Motion in the M87 Jet”. *ApJ*, 520, 621
- Biretta, J. A., Zhou, F., and Owen, F. N. 1995, “Detection of Proper Motions in the M87 Jet”. *ApJ*, 447, 582
- Blandford, R. D. and Rees, M. J. 1974, “A ‘twin-exhaust’ model for double radio sources”. *MNRAS*, 169, 395
- Bogovalov, S. and Tsinganos, K. 2005, “Shock formation at the magnetic collimation of relativistic jets”. *MNRAS*, 357, 918
- Bower, G. C., Falcke, H., Herrnstein, R. M., et al. 2004, “Detection of the Intrinsic Size of Sagittarius A* Through Closure Amplitude Imaging”. *Science*, 304, 704
- Bower, G. C., Goss, W. M., Falcke, H., et al. 2006, “The Intrinsic Size of Sagittarius A* from 0.35 to 6 cm”. *ApJ*, 648, L127
- Braatz, J., Greenhill, L., Moran, J., et al., “A VLBA Map of the H₂O Maser in the Nucleus of Seyfert 2 Galaxy NGC 1386”, in: M. F. Bietenholz, N. Bartel, M. P. Rupen, A. J. Beasley, D. A. Graham, V. I. Altunin, T. Venturi, G. Umana, and J. E. Conway (eds.), *Bulletin of the American Astronomical Society*, vol. 29 of *Bulletin of the American Astronomical Society*, p. 1374 (1997)

- Braatz, J. A., Henkel, C., Greenhill, L. J., et al. 2004, “A Green Bank Telescope Search for Water Masers in Nearby Active Galactic Nuclei”. *ApJ*, 617, L29
- Braatz, J. A., Wilson, A. S., and Henkel, C. 1996, “A Survey for H₂O Megamasers in Active Galactic Nuclei. I. Observations”. *ApJS*, 106, 51
- Bradač, M., Schneider, P., Steinmetz, M., et al. 2002, “B1422+231: The influence of mass substructure on strong lensing”. *A&A*, 388, 373
- Bradshaw, C. F., Fomalont, E. B., and Geldzahler, B. J. 1999, “High-Resolution Parallax Measurements of Scorpius X-1”. *ApJ*, 512, L121
- Bridle, A. H. and Perley, R. A. 1984, “Extragalactic Radio Jets”. *ARA&A*, 22, 319
- Brisken, W. F., Benson, J. M., Goss, W. M., et al. 2002, “Very Long Baseline Array Measurement of Nine Pulsar Parallaxes”. *ApJ*, 571, 906
- Brown, R. L. 1982, “Precessing jets in Sagittarius A - Gas dynamics in the central parsec of the galaxy”. *ApJ*, 262, 110
- Brunthaler, A., Falcke, H., Bower, G. C., et al. 2000, “III Zw 2, the first superluminal jet in a Seyfert galaxy”. *A&A*, 357, L45
- Brunthaler, A., Reid, M. J., Falcke, H., et al. 2005, “The Geometric Distance and Proper Motion of the Triangulum Galaxy (M33)”. *Science*, 307, 1440
- Brunthaler, A., Reid, M. J., Falcke, H., et al. 2007, “The proper motion of the Local Group galaxy IC 10”. *A&A*, 462, 101
- Burn, B. J. 1966, “On the depolarization of discrete radio sources by Faraday dispersion”. *MNRAS*, 133, 67
- Capetti, A. and Balmaverde, B. 2006, “The host galaxy/AGN connection in nearby early-type galaxies. A new view of the origin of the radio-quiet/radio-loud dichotomy?” *A&A*, 453, 27
- Carilli, C. and Rawlings, S. (eds.), *Science with the Square Kilometre Array* (Elsevier, 2004)
- Carilli, C. L., “VLBI with the Square Kilometer Array”, in: J. Romney and M. Reid (eds.), *Future Directions in High Resolution Astronomy*, vol. 340 of *Astronomical Society of the Pacific Conference Series*, p. 560 (2005)
- Carlip, S. 2004, “Model-dependence of Shapiro time delay and the ‘speed of gravity/speed of light’ controversy”. *Classical and Quantum Gravity*, 21, 3803
- Carlip, S. 2005, “COMMENTS, REPLIES AND NOTES: Reply to the comment on ‘Model dependence of Shapiro time delay and the ‘speed of gravity/speed of light’ controversy’”. *Classical and Quantum Gravity*, 22, 5187

- Carrara, E. A., Abraham, Z., Unwin, S. C., et al. 1993, “The milliarcsecond structure of the quasar 3C 279”. *A&A*, 279, 83
- Cawthorne, T. V. 2006, “Polarization of synchrotron radiation from conical shock waves”. *MNRAS*, 367, 851
- Cawthorne, T. V., Wardle, J. F. C., Roberts, D. H., et al. 1993, “Milliarcsecond Polarization Structure of 24 Objects from the Pearson-Readhead Sample of Bright Extragalactic Radio Sources. II. Discussion”. *ApJ*, 416, 519
- Celotti, A. and Fabian, A. C. 1993, “The Kinetic Power and Luminosity of Parsecscale Radio Jets - an Argument for Heavy Jets”. *MNRAS*, 264, 228
- Chatterjee, S., Vlemmings, W. H. T., Briske, W. F., et al. 2005, “Getting Its Kicks: A VLBA Parallax for the Hyperfast Pulsar B1508+55”. *ApJ*, 630, L61
- Chevalier, R. A. 1982, “Self-similar solutions for the interaction of stellar ejecta with an external medium”. *ApJ*, 258, 790
- Clark, B. G., “Coherence in Radio Astronomy”, in: G. B. Taylor, C. L. Carilli, and R. A. Perley (eds.), *ASP Conf. Ser. 180: Synthesis Imaging in Radio Astronomy II*, p. 1 (1999)
- Claussen, M. J., Goss, W. M., Frail, D. A., et al. 1999, “The Sizes of 1720 MHz OH Masers: VLBA and MERLIN Observations of the Supernova Remnants W44 and W28”. *ApJ*, 522, 349
- Cohen, M. H., Linfield, R. P., Moffet, A. T., et al. 1977, “Radio sources with superluminal velocities”. *Nature*, 268, 405
- Cohen, M. H., Lister, M. L., Homan, D. C., et al. 2007, “Relativistic Beaming and the Intrinsic Properties of Extragalactic Radio Jets”. *ApJ*, 658, 232
- Conway, J. E., “HI Absorption from a Circumnuclear TORUS in the Hidden Quasar Cygnus A”, in: C. L. Carilli, S. J. E. Radford, K. M. Menten, and G. I. Langston (eds.), *Highly Redshifted Radio Lines*, vol. 156 of *Astronomical Society of the Pacific Conference Series*, p. 259 (1999a)
- Conway, J. E. 1999b, “VLBI spectral absorption in AGN”. *New Astronomy Review*, 43, 509
- Cornwell, T. and Fomalont, E. B., “Self-Calibration”, in: G. B. Taylor, C. L. Carilli, and R. A. Perley (eds.), *Synthesis Imaging in Radio Astronomy II*, vol. 180 of *Astronomical Society of the Pacific Conference Series*, p. 187 (1999)
- Cotton, W. D., “Fringe Fitting”, in: J. A. Zensus, P. J. Diamond, and P. J. Napier (eds.), *Very Long Baseline Interferometry and the VLBA*, vol. 82 of *Astronomical Society of the Pacific Conference Series*, p. 189 (1995)

- Cotton, W. D., Geldzahler, B. J., Marcaide, J. M., et al. 1984, “VLBI observations of the polarized radio emission from the quasar 3C 454.3”. *ApJ*, 286, 503
- Cotton, W. D., Vlemmings, W., Mennesson, B., et al. 2006, “Further VLBA observations of SiO masers toward Mira variable stars”. *A&A*, 456, 339
- Cotton, W. D., Wittels, J. J., Shapiro, I. I., et al. 1980, “The very flat radio spectrum of 0735 plus 178 - A cosmic conspiracy”. *ApJ*, 238, L123
- Daly, R. A. and Marscher, A. P. 1988, “The gasdynamics of compact relativistic jets”. *ApJ*, 334, 539
- Deller, A. T., Tingay, S. J., Bailes, M., et al. 2007, “DiFX: A Software Correlator for Very Long Baseline Interferometry Using Multiprocessor Computing Environments”. *PASP*, 119, 318
- Dennett-Thorpe, J. and de Bruyn, A. G. 2002, “Interstellar scintillation as the origin of the rapid radio variability of the quasar J1819+3845”. *Nature*, 415, 57
- Dennett-Thorpe, J. and de Bruyn, A. G. 2003, “Annual modulation in the scattering of J1819+3845: Peculiar plasma velocity and anisotropy”. *A&A*, 404, 113
- Dent, W. A. 1965, “Quasi-Stellar Sources: Variation in the Radio Emission of 3C 273”. *Science*, 148, 1458
- Dhawan, V., Mirabel, I. F., and Rodríguez, L. F. 2000, “AU-Scale Synchrotron Jets and Superluminal Ejecta in GRS 1915+105”. *ApJ*, 543, 373
- Dhawan, V. and Rupen, M., “LS I +61 303 is a Be-Pulsar binary, not a Microquasar”, in: VI Microquasar Workshop: Microquasars and Beyond (2006)
- Diamond, P. J. and Kemball, A. J. 2003, “A Movie of a Star: Multiepoch Very Long Baseline Array Imaging of the SiO Masers toward the Mira Variable TX Cam”. *ApJ*, 599, 1372
- Dodson, R., Edwards, P. G., and Hirabayashi, H. 2006, “Milliarcsecond-Scale Spectral Properties and Jet Motions in M 87”. *PASJ*, 58, 243
- Dodson, R., Legge, D., Reynolds, J. E., et al. 2003, “The Vela Pulsar’s Proper Motion and Parallax Derived from VLBI Observations”. *ApJ*, 596, 1137
- Doeleman, S. S., Shen, Z.-Q., Rogers, A. E. E., et al. 2001, “Structure of Sagittarius A* at 86 GHz using VLBI Closure Quantities”. *AJ*, 121, 2610
- Dyson, F. W., Eddington, A. S., and Davidson, C. 1920. *Philos. Trans. R. Soc.*, 220, 291

- Eckart, A. and Genzel, R. 1996, “Observations of stellar proper motions near the Galactic Centre”. *Nature*, 383, 415
- Eckart, A. and Genzel, R. 1997, “Stellar proper motions in the central 0.1 PC of the Galaxy”. *MNRAS*, 284, 576
- Edwards, P. G. and Piner, B. G. 2002, “The Subluminal Parsec-Scale Jet of Markarian 501”. *ApJ*, 579, L67
- Eisenhauer, F., Schödel, R., Genzel, R., et al. 2003, “A Geometric Determination of the Distance to the Galactic Center”. *ApJ*, 597, L121
- Falcke, H., “The Silent Majority – Jets and Radio Cores from Low-Luminosity Black Holes”, in: R. E. Schielicke (ed.), *Reviews in Modern Astronomy*, vol. 14 of *Reviews in Modern Astronomy*, p. 15 (2001)
- Falcke, H., Mannheim, K., and Biermann, P. L. 1993, “The Galactic Center radio jet”. *A&A*, 278, L1
- Falcke, H., Melia, F., and Agol, E. 2000, “Viewing the Shadow of the Black Hole at the Galactic Center”. *ApJ*, 528, L13
- Falcke, H., Patnaik, A. R., and Sherwood, W. 1996a, “EVN + MERLIN Observations of Radio-intermediate Quasars: Evidence for Boosted Radio-weak Quasars”. *ApJ*, 473, L13
- Falcke, H., Sherwood, W., and Patnaik, A. R. 1996b, “The Nature of Radio-intermediate Quasars: What Is Radio-loud and What Is Radio-quiet?” *ApJ*, 471, 106
- Fanaroff, B. L. and Riley, J. M. 1974, “The morphology of extragalactic radio sources of high and low luminosity”. *MNRAS*, 167, 31
- Faraday, M., *Faraday’s Diary*, vol. 4 (, ed. T. Martin, (London: Bell & Sons), 1933), p. 264
- Feissel, M. and Mignard, F. 1998, “The adoption of ICRS on 1 January 1998: meaning and consequences”. *A&A*, 331, L33
- Fomalont, E. B., Frey, S., Paragi, Z., et al. 2000, “The VSOP 5 GHz Continuum Survey: The Prelaunch VLBA Observations”. *ApJS*, 131, 95
- Fomalont, E. B., Geldzahler, B. J., and Bradshaw, C. F. 2001, “Scorpius X-1: The Evolution and Nature of the Twin Compact Radio Lobes”. *ApJ*, 558, 283
- Fomalont, E. B. and Kopeikin, S. M. 2003, “The Measurement of the Light Deflection from Jupiter: Experimental Results”. *ApJ*, 598, 704
- Fricke, W., Schwan, H., Lederle, T., et al. 1988, “Fifth fundamental catalogue (FK5). Part 1: The basic fundamental stars”. *Veroeffentlichungen des Astronomischen Rechen-Instituts Heidelberg*, 32, 1

- Gabányi, K. É., Marchili, N., Krichbaum, T. P., et al. 2007, “The IDV source J 1128+5925, a new candidate for annual modulation?” *A&A*, 470, 83
- Gabuzda, D. C. and Cawthorne, T. V. 1996, “The parsec-scale polarization structure of nine BL Lacertae objects at $\lambda=3.6\text{cm}$ ”. *MNRAS*, 283, 759
- Gabuzda, D. C. and Gómez, J. L. 2001, “VSOP polarization observations of the BL Lacertae object OJ 287”. *MNRAS*, 320, L49
- Gabuzda, D. C., Pushkarev, A. B., and Cawthorne, T. V. 2000, “Analysis of $\lambda=6\text{cm}$ VLBI polarization observations of a complete sample of northern BL Lacertae objects”. *MNRAS*, 319, 1109
- Garrett, M. A., Muxlow, T. W. B., Garrington, S. T., et al. 2001, “AGN and starbursts at high redshift: High resolution EVN radio observations of the Hubble Deep Field”. *A&A*, 366, L5
- Garrett, M. A., Wrobel, J. M., and Morganti, R. 2005, “Deep VLBI Imaging of Faint Radio Sources in the NOAO Bootes Field”. *ApJ*, 619, 105
- Genzel, R., Reid, M. J., Moran, J. M., et al. 1981, “Proper motions and distances of H_2O maser sources. I - The outflow in Orion-KL”. *ApJ*, 244, 884
- Ghez, A. M., Klein, B. L., Morris, M., et al. 1998, “High Proper-Motion Stars in the Vicinity of Sagittarius A*: Evidence for a Supermassive Black Hole at the Center of Our Galaxy”. *ApJ*, 509, 678
- Ghez, A. M., Salim, S., Hornstein, S. D., et al. 2005, “Stellar Orbits around the Galactic Center Black Hole”. *ApJ*, 620, 744
- Gómez, J.-L., Marscher, A. P., Alberdi, A., et al. 2001, “Monthly 43 GHz VLBA Polarimetric Monitoring of 3C 120 over 16 Epochs: Evidence for Trailing Shocks in a Relativistic Jet”. *ApJ*, 561, L161
- Gomez, J. L., Marti, J. M. A., Marscher, A. P., et al. 1995, “Parsec-Scale Synchrotron Emission from Hydrodynamic Relativistic Jets in Active Galactic Nuclei”. *ApJ*, 449, L19
- Gower, A. C., Gregory, P. C., Unruh, W. G., et al. 1982, “Relativistic precessing jets in quasars and radio galaxies - Models to fit high resolution data”. *ApJ*, 262, 478
- Greenhill, L. J., Booth, R. S., Ellingsen, S. P., et al. 2003a, “A Warped Accretion Disk and Wide-Angle Outflow in the Inner Parsec of the Circinus Galaxy”. *ApJ*, 590, 162
- Greenhill, L. J. and Gwinn, C. R. 1997, “VLBI Imaging of Water Maser Emission from a Nuclear Disk in NGC 1068”. *Ap&SS*, 248, 261

- Greenhill, L. J., Kondratko, P. T., Lovell, J. E. J., et al. 2003b, “The Discovery of H₂O Maser Emission in Seven Active Galactic Nuclei and at High Velocities in the Circinus Galaxy”. *ApJ*, 582, L11
- Greenhill, L. J., Moran, J. M., and Herrnstein, J. R. 1997, “The Distribution of H₂O Maser Emission in the Nucleus of NGC 4945”. *ApJ*, 481, L23+
- Greve, A., Könönen, P., Graham, D. A., et al. 2002, “147 GHz VLBI observations: Detection of 3C 273 and 3C 279 on the 3100 km baseline Metsähovi - Pico Veleta”. *A&A*, 390, L19
- Högbom, J. A. 1974, “Aperture Synthesis with a Non-Regular Distribution of Interferometer Baselines”. *A&AS*, 15, 417
- Hagiwara, Y., Diamond, P. J., and Miyoshi, M. 2002, “A search for extragalactic H₂O maser emission towards IRAS galaxies. Detection of a maser from an infrared-luminous merger, NGC 6240”. *A&A*, 383, 65
- Hall, P. J., *The Square Kilometre Array: An Engineering Perspective* (Berlin: Springer, 2005., 2005)
- Hardee, P. E. 2003, “Modeling Helical Structures in Relativistic Jets”. *ApJ*, 597, 798
- Heeschen, D. S., Krichbaum, T. P., Schalinski, C. J., et al. 1987, “Rapid variability of extragalactic radio sources”. *AJ*, 94, 1493
- Helfand, D. J., Chatterjee, S., Briskin, W. F., et al. 2007, “VLBA Measurement of the Transverse Velocity of the Magnetar XTE J1810-197”. *ApJ*, 662, 1198
- Helmboldt, J. F., Taylor, G. B., Tremblay, S., et al. 2007, “The VLBA Imaging and Polarimetry Survey at 5 GHz”. *ApJ*, 658, 203
- Henkel, C., Peck, A. B., Tarchi, A., et al. 2005, “New H₂O masers in Seyfert and FIR bright galaxies”. *A&A*, 436, 75
- Herrnstein, J. R., Moran, J. M., Greenhill, L. J., et al. 1999, “A geometric distance to the galaxy NGC4258 from orbital motions in a nuclear gas disk”. *Nature*, 400, 539
- Herrnstein, J. R., Moran, J. M., Greenhill, L. J., et al. 2005, “The Geometry of and Mass Accretion Rate through the Maser Accretion Disk in NGC 4258”. *ApJ*, 629, 719
- Hirabayashi, H., Hirose, H., Kobayashi, H., et al. 2000, “The VLBI Space Observatory Programme and the Radio-Astronomical Satellite HALCA”. *PASJ*, 52, 955
- Hirota, T., Bushimata, T., Choi, Y. K., et al. 2007a, “Astrometry of Water Maser Sources in Nearby Molecular Clouds with VERA - II. SVS 13 in NGC 1333”. *ArXiv e-prints*, 709

- Hirota, T., Bushimata, T., Choi, Y. K., et al. 2007b, “Distance to Orion KL Measured with VERA”. ArXiv e-prints, 705
- Hoffman, I. M., Goss, W. M., Brogan, C. L., et al. 2005, “The OH (1720 MHz) Supernova Remnant Masers in W28: MERLIN and VLBA Polarization Observations”. *ApJ*, 620, 257
- Homan, D. C., Attridge, J. M., and Wardle, J. F. C. 2001, “Parsec-Scale Circular Polarization Observations of 40 Blazars”. *ApJ*, 556, 113
- Homan, D. C. and Lister, M. L. 2006, “MOJAVE: Monitoring of Jets in Active Galactic Nuclei with VLBA Experiments. II. First-Epoch 15 GHz Circular Polarization Results”. *AJ*, 131, 1262
- Homan, D. C. and Wardle, J. F. C. 1999, “Detection and Measurement of Parsec-Scale Circular Polarization in Four AGNS”. *AJ*, 118, 1942
- Homan, D. C. and Wardle, J. F. C. 2003, “Probing the Circular Polarization of Relativistic Jets on VLBI Scales”. *Ap&SS*, 288, 29
- Homan, D. C. and Wardle, J. F. C. 2004, “High Levels of Circularly Polarized Emission from the Radio Jet in NGC 1275 (3C 84)”. *ApJ*, 602, L13
- Honma, M., Bushimata, T., Choi, Y. K., et al. 2007, “Astrometry of Galactic Star Forming Region Sharpless 269 with VERA : Parallax Measurements and Constraint on Outer Rotation Curve”. ArXiv e-prints, 709
- Horiuchi, S., Fomalont, E. B., Taylor, W. K., et al. 2004, “The VSOP 5 GHz Active Galactic Nucleus Survey. IV. The Angular Size/Brightness Temperature Distribution”. *ApJ*, 616, 110
- Horiuchi, S., Meier, D. L., Preston, R. A., et al. 2006, “Ten Milliparsec-Scale Structure of the Nucleus Region in Centaurus A”. *PASJ*, 58, 211
- Hughes, P. A., Aller, H. D., and Aller, M. F. 1985, “Polarized Radio Outbursts in BL-Lacertae - Part Two - the Flux and Polarization of a Piston-Driven Shock”. *ApJ*, 298, 301
- Hughes, P. A., Aller, H. D., and Aller, M. F. 1989, “Synchrotron emission from shocked relativistic jets. I - The theory of radio-wavelength variability and its relation to superluminal motion”. *ApJ*, 341, 54
- Hughes, P. A., Miller, M. A., and Duncan, G. C. 2002, “Three-dimensional Hydrodynamic Simulations of Relativistic Extragalactic Jets”. *ApJ*, 572, 713
- Hummel, C. A., Schalinski, C. J., Krichbaum, T. P., et al. 1992, “The jets of quasar 1928+738 - Superluminal motion and large-scale structure”. *A&A*, 257, 489
- Imai, H., Horiuchi, S., Deguchi, S., et al. 2003, “Linear Polarization Observations of Water Masers in W3 IRS 5”. *ApJ*, 595, 285

- Ishihara, Y., Nakai, N., Iyomoto, N., et al. 2001, “Water-Vapor Maser Emission from the Seyfert 2 Galaxy IC 2560: Evidence for a Super-Massive Black Hole”. PASJ, 53, 215
- Jones, D. L., Wehrle, A. E., Piner, B. G., et al. 2001, “In the Shadow of the Accretion Disk: Higher Resolution Imaging of the Central Parsec in NGC 4261”. ApJ, 553, 968
- Jones, T. W. and O’dell, S. L. 1977, “Physical conditions in polarized compact radio sources”. A&A, 61, 291
- Jorstad, S. G., Marscher, A. P., Lister, M. L., et al. 2005, “Polarimetric Observations of 15 Active Galactic Nuclei at High Frequencies: Jet Kinematics from Bimonthly Monitoring with the Very Long Baseline Array”. AJ, 130, 1418
- Jorstad, S. G., Marscher, A. P., Mattox, J. R., et al. 2001a, “Multiepoch Very Long Baseline Array Observations of EGRET-detected Quasars and BL Lacertae Objects: Connection between Superluminal Ejections and Gamma-Ray Flares in Blazars”. ApJ, 556, 738
- Jorstad, S. G., Marscher, A. P., Mattox, J. R., et al. 2001b, “Multiepoch Very Long Baseline Array Observations of EGRET-detected Quasars and BL Lacertae Objects: Superluminal Motion of Gamma-Ray Bright Blazars”. ApJS, 134, 181
- Jorstad, S. G., Marscher, A. P., Stevens, J. A., et al. 2007, “Multiwaveband Polarimetric Observations of 15 Active Galactic Nuclei at High Frequencies: Correlated Polarization Behavior”. AJ, 134, 799
- Junor, W., Biretta, J. A., and Livio, M. 1999, “Formation of the radio jet in M87 at 100 Schwarzschild radii from the central black hole”. Nature, 401, 891
- Kedziora-Chudczer, L. L., Jauncey, D. L., Wieringa, M. H., et al. 2001, “The ATCA intraday variability survey of extragalactic radio sources”. MNRAS, 325, 1411
- Kellermann, K. I. 2002, “Brightness Temperature Constraints to Compact Synchrotron Source Radiation Obtained from IDV and VLBI Observations”. Publications of the Astronomical Society of Australia, 19, 77
- Kellermann, K. I., “Variability, Brightness Temperature, Superluminal Motion, Doppler Boosting, and Related Issues”, in: J. A. Zensus, M. H. Cohen, and E. Ros (eds.), Radio Astronomy at the Fringe, vol. 300 of Astronomical Society of the Pacific Conference Series, p. 185 (2003)
- Kellermann, K. I., Lister, M. L., Homan, D. C., et al. 2004, “Sub-Milliarcsecond Imaging of Quasars and Active Galactic Nuclei. III. Kinematics of Parsec-scale Radio Jets”. ApJ, 609, 539

- Kellermann, K. I. and Moran, J. M. 2001, “The Development of High-Resolution Imaging in Radio Astronomy”. *ARA&A*, 39, 457
- Kellermann, K. I. and Pauliny-Toth, I. I. K. 1969, “The Spectra of Opaque Radio Sources”. *ApJ*, 155, L71
- Kellermann, K. I., Sramek, R. A., Schmidt, M., et al. 1994, “The radio structure of radio loud and radio quiet quasars in the Palomar Bright Quasar Survey”. *AJ*, 108, 1163
- Kellermann, K. I., Vermeulen, R. C., Zensus, J. A., et al. 1998, “Sub-Milliarcsecond Imaging of Quasars and Active Galactic Nuclei”. *AJ*, 115, 1295
- Kemball, A., Flatters, C., Gabuzda, D., et al. 2000, “VSOP Polarization Observing at 1.6 GHz and 5 GHz”. *PASJ*, 52, 1055
- Kemball, A. J., “VLBI polarimetry”, in: G. B. Taylor, C. L. Carilli, and R. A. Perley (eds.), *Synthesis Imaging in Radio Astronomy II*, vol. 180 of *Astronomical Society of the Pacific Conference Series*, p. 499 (1999)
- Komesaroff, M. M., Roberts, J. A., Milne, D. K., et al. 1984, “Circular and linear polarization variations of compact radio sources”. *MNRAS*, 208, 409
- Kondratko, P. T., Greenhill, L. J., and Moran, J. M. 2005, “Evidence for a Geometrically Thick Self-Gravitating Accretion Disk in NGC 3079”. *ApJ*, 618, 618
- Kondratko, P. T., Greenhill, L. J., Moran, J. M., et al. 2006, “Discovery of Water Maser Emission in Eight AGNs with 70 m Antennas of NASA’s Deep Space Network”. *ApJ*, 638, 100
- Königl, A. 1981, “Relativistic jets as X-ray and gamma-ray sources”. *ApJ*, 243, 700
- Koopmans, L. V. E., Garrett, M. A., Blandford, R. D., et al. 2002, “2016+112: a gravitationally lensed type II quasar”. *MNRAS*, 334, 39
- Kopeikin, S. M. 2005, “COMMENTS, REPLIES AND NOTES: Comment on ‘Model-dependence of Shapiro time delay and the “speed of gravity/speed of light” controversy’”. *Classical and Quantum Gravity*, 22, 5181
- Kovalev, Y. Y., Lister, M. L., Homan, D. C., et al. 2007, “The Inner Jet of the Radio Galaxy M87”. *ApJ*, 668, L27
- Kraus, A., Krichbaum, T. P., Wegner, R., et al. 2003, “Intraday variability in compact extragalactic radio sources. II. Observations with the Effelsberg 100 m radio telescope”. *A&A*, 401, 161
- Kraus, A., Krichbaum, T. P., and Witzel, A., “Intraday Variability in BL Lac Objects and Quasars”, in: L. Takalo and A. Sillanpää (eds.), *BL Lac Phenomenon*, no. 159 in *ASP Conf. Ser.*, p. 49 (ASP, San Francisco, CA, 1999a)

- Kraus, A., Witzel, A., and Krichbaum, T. P. 1999b, “Intraday radio variability in active galactic nuclei”. *New Astronomy Review*, 43, 685
- Krichbaum, T. P., Alef, W., Witzel, A., et al. 1998a, “VLBI observations of CygnusA with sub-milliarcsecond resolution”. *A&A*, 329, 873
- Krichbaum, T. P., Graham, D. A., Alef, W., et al., “VLBI observations at 147 GHz: first detection of transatlantic fringes in bright AGN”, in: E. Ros, R. W. Porcas, A. P. Lobanov, and J. A. Zensus (eds.), *Proceedings of the 6th EVN Symposium*, p. 125 (MPiR, Bonn, Germany, 2002a)
- Krichbaum, T. P., Graham, D. A., Alef, W., et al., “Towards the Event Horizon - The Vicinity of AGN at Micro-Arcsecond Resolution”, in: R. Bachiller, F. Colomer, J.-F. Desmurs, and P. de Vicente (eds.), *European VLBI Network on New Developments in VLBI Science and Technology*, pp. 15–18 (2004)
- Krichbaum, T. P., Graham, D. A., Bremer, M., et al. 2006, “Sub-Milliarcsecond Imaging of Sgr A* and M 87”. *Journal of Physics Conference Series*, 54, 328
- Krichbaum, T. P., Graham, D. A., Witzel, A., et al. 1998b, “VLBI observations of the galactic center source SGR A* at 86 GHz and 215 GHz”. *A&A*, 335, L106
- Krichbaum, T. P., Kraus, A., Fuhrmann, L., et al. 2002b, “Intraday Variability in Northern Hemisphere Radio Sources”. *Publications of the Astronomical Society of Australia*, 19, 14
- Laing, R. A. and Bridle, A. H. 2002, “Relativistic models and the jet velocity field in the radio galaxy 3C 31”. *MNRAS*, 336, 328
- Laing, R. A., Parma, P., de Ruiter, H. R., et al. 1999, “Asymmetries in the jets of weak radio galaxies”. *MNRAS*, 306, 513
- Lenc, E., Garrett, M. A., Wucknitz, O., et al. 2006, “Living life on the edge - Wide-field VLBI at 90 cm!” *astro-ph/0612618*
- Lenc, E. and Tingay, S. J. 2006, “The Subparsec-Scale Radio Properties of Southern Starburst Galaxies. I. Supernova Remnants, the Supernova Rate, and the Ionized Medium in the NGC 253 Starburst”. *AJ*, 132, 1333
- Leppänen, K., Liljeström, T., and Diamond, P. 1998, “Submilliarcsecond Linear Polarization Observations of Water Masers in W51 M”. *ApJ*, 507, 909
- Leppänen, K. J., Zensus, J. A., and Diamond, P. J. 1995, “Linear Polarization Imaging with Very Long Baseline Interferometry at High Frequencies”. *AJ*, 110, 2479
- Lestrade, J.-F., Preston, R. A., Jones, D. L., et al. 1999, “High-precision VLBI astrometry of radio-emitting stars”. *A&A*, 344, 1014

- Lister, M. L., “The MOJAVE Program: Studying the Relativistic Kinematics of AGN Jets”, in: J. D. Romney and M. J. Reid (eds.), ASP Conf. Ser. 340: Future Directions in High Resolution Astronomy, p. 20 (ASP, San Francisco, CA, 2005)
- Lister, M. L. and Homan, D. C. 2005, “MOJAVE: Monitoring of Jets in Active Galactic Nuclei with VLBA Experiments. I. First-Epoch 15 GHz Linear Polarization Images”. *AJ*, 130, 1389
- Lister, M. L. and Smith, P. S. 2000, “Intrinsic Differences in the Inner Jets of High and Low Optically Polarized Radio Quasars”. *ApJ*, 541, 66
- Lister, M. L., Tingay, S. J., and Preston, R. A. 2001, “The Pearson-Readhead Survey of Compact Extragalactic Radio Sources from Space. II. Analysis of Source Properties”. *ApJ*, 554, 964
- Lo, K. Y., Shen, Z.-Q., Zhao, J.-H., et al. 1998, “Intrinsic Size of Sagittarius A*: 72 Schwarzschild Radii”. *ApJ*, 508, L61
- Lobanov, A., Hardee, P., and Eilek, J. 2003, “Internal structure and dynamics of the kiloparsec-scale jet in M87”. *New Astronomy Review*, 47, 629
- Lobanov, A. P. 1998a, “Spectral distributions in compact radio sources. I. Imaging with VLBI data”. *A&AS*, 132, 261
- Lobanov, A. P. 1998b, “Ultracompact jets in active galactic nuclei”. *A&A*, 330, 79
- Lobanov, A. P., Krichbaum, T. P., Witzel, A., et al. 2006, “Dual-Frequency VSOP Imaging of the Jet in S5 0836+710”. *PASJ*, 58, 253
- Lobanov, A. P. and Roland, J. 2005, “A supermassive binary black hole in the quasar 3C 345”. *A&A*, 431, 831
- Lobanov, A. P. and Zensus, J. A. 1999, “Spectral Evolution of the Parsec-Scale Jet in the Quasar 3C 345”. *ApJ*, 521, 509
- Lobanov, A. P. and Zensus, J. A. 2001, “A Cosmic Double Helix in the Archetypical Quasar 3C273”. *Science*, 294, 128
- Loeb, A., Reid, M. J., Brunthaler, A., et al. 2005, “Constraints on the Proper Motion of the Andromeda Galaxy Based on the Survival of Its Satellite M33”. *ApJ*, 633, 894
- Loinard, L., Torres, R. M., Mioduszewski, A. J., et al. 2007, “VLBA determination of the distance to nearby star-forming regions I. The distance to T Tauri with 0.4% accuracy”. *ArXiv e-prints*, 708
- Lonsdale, C. J., Diamond, P. J., Thrall, H., et al. 2006, “VLBI Images of 49 Radio Supernovae in Arp 220”. *ApJ*, 647, 185

- Lovell, J. E. J., Jauncey, D. L., Bignall, H. E., et al. 2003, “First Results from MASIV: The Microarcsecond Scintillation-induced Variability Survey”. *AJ*, 126, 1699
- Ly, C., Walker, R. C., and Junor, W. 2007, “High-Frequency VLBI Imaging of the Jet Base of M87”. *ApJ*, 660, 200
- Lynden-Bell, D. and Rees, M. J. 1971, “On quasars, dust and the galactic centre”. *MNRAS*, 152, 461
- Lyutikov, M., Pariev, V. I., and Gabuzda, D. C. 2005, “Polarization and structure of relativistic parsec-scale AGN jets”. *MNRAS*, 360, 869
- Ma, C., Arias, E. F., Eubanks, T. M., et al. 1998, “The International Celestial Reference Frame as Realized by Very Long Baseline Interferometry”. *AJ*, 116, 516
- Macchetto, F., Marconi, A., Axon, D. J., et al. 1997, “The Supermassive Black Hole of M87 and the Kinematics of Its Associated Gaseous Disk”. *ApJ*, 489, 579
- Marcaide, J. M., Alberdi, A., Ros, E., et al. 1995a, “Discovery of Shell-Like Radio-Structure in Supernova 1993J”. *Nature*, 373, 44
- Marcaide, J. M., Alberdi, A., Ros, E., et al. 1995b, “Expansion of Supernova 1993J”. *Science*, 270, 1475
- Marcaide, J. M., Alberdi, A., Ros, E., et al. 1997, “Deceleration in the Expansion of SN 1993J”. *ApJ*, 486, L31
- Marcaide, J. M., Rogers, A. E. E., Alberdi, A., et al. 1993, “Supernova 1993J in NGC 3031”. *IAU Circ.*, 5785, 2
- Marscher, A. P. 1977, “Structure of radio sources with remarkably flat spectra - PKS 0735+178”. *AJ*, 82, 781
- Marscher, A. P., “Multiband Impressions of Active Galactic Nuclei”, in: A. Lobanov and T. Venturi (eds.), *Multiband Approach to AGN* held in Sept. 2004, Bonn, Germany, vol. 76, p. 168 (*Mem. Soc. Astron. It.*, 2005a)
- Marscher, A. P., “Relationship between High-Frequency Emission and the Radio Jet in Blazars”, in: J. Romney and M. Reid (eds.), *Future Directions in High Resolution Astronomy*, vol. 340 of *Astronomical Society of the Pacific Conference Series*, p. 25 (2005b)
- Marscher, A. P. and Gear, W. K. 1985, “Models for high-frequency radio outbursts in extragalactic sources, with application to the early 1983 millimeter-to-infrared flare of 3C 273”. *ApJ*, 298, 114
- Marscher, A. P., Jorstad, S. G., Gómez, J. L., et al. 2007, “Search for Electron-Positron Annihilation Radiation from the Jet in 3C 120”. *ApJ*, 665, 232

- Marscher, A. P., Jorstad, S. G., Mattox, J. R., et al. 2002, “High-Frequency VLBA Total and Polarized Intensity Images of Gamma-Ray Bright Blazars”. *ApJ*, 577, 85
- McDonald, A. R., Muxlow, T. W. B., Pedlar, A., et al. 2001, “Global very long-baseline interferometry observations of compact radio sources in M82”. *MNRAS*, 322, 100
- Meier, D. L., Koide, S., and Uchida, Y. 2001, “Magnetohydrodynamic Production of Relativistic Jets”. *Science*, 291, 84
- Melia, F. 1994, “An accreting black hole model for Sagittarius A*. 2: A detailed study”. *ApJ*, 426, 577
- Melia, F. and Falcke, H. 2001, “The Supermassive Black Hole at the Galactic Center”. *ARA&A*, 39, 309
- Middelberg, E., Agudo, I., Roy, A. L., et al. 2007, “Jet-cloud collisions in the jet of the Seyfert galaxy NGC3079”. *MNRAS*, 377, 731
- Miller-Jones, J. C. A., Blundell, K. M., Rupen, M. P., et al. 2004, “Time-sequenced Multi-Radio Frequency Observations of Cygnus X-3 in Flare”. *ApJ*, 600, 368
- Mioduszewski, A. J., Rupen, M. P., Walker, R. C., et al., “A Summer of SS433: Forty Days of VLBA Imaging”, in: *Bulletin of the American Astronomical Society*, vol. 36 of *Bulletin of the American Astronomical Society*, p. 967 (2004)
- Mirabel, I. F. 2006, “Very energetic gamma-rays from microquasars and binary pulsars”. *Science*, 312, 1759
- Miyoshi, M., Moran, J., Herrnstein, J., et al. 1995, “Evidence for a Black-Hole from High Rotation Velocities in a Sub-Parsec Region of NGC4258”. *Nature*, 373, 127
- Mundell, C. G., Pedlar, A., Baum, S. A., et al. 1995, “MERLIN observations of neutral hydrogen absorption in the Seyfert nucleus of NGC 4151”. *MNRAS*, 272, 355
- Mundell, C. G., Wrobel, J. M., Pedlar, A., et al. 2003, “The Nuclear Regions of the Seyfert Galaxy NGC 4151: Parsec-Scale H I Absorption and a Remarkable Radio Jet”. *ApJ*, 583, 192
- Nagar, N. M., Falcke, H., Wilson, A. S., et al. 2002, “Radio sources in low-luminosity active galactic nuclei. III. “AGNs” in a distance-limited sample of “LLAGNs””. *A&A*, 392, 53
- Narayan, R., Mahadevan, R., Grindlay, J. E., et al. 1998, “Advection-dominated accretion model of Sagittarius A*: evidence for a black hole at the Galactic center.” *ApJ*, 492, 554

- Neff, S. G., Ulvestad, J. S., and Teng, S. H. 2004, “A Supernova Factory in the Merger System Arp 299”. *ApJ*, 611, 186
- Neufeld, D. A., Maloney, P. R., and Conger, S. 1994, “Water maser emission from X-ray-heated circumnuclear gas in active galaxies”. *ApJ*, 436, L127
- Ng, C.-Y., Romani, R. W., Briskin, W. F., et al. 2007, “The Origin and Motion of PSR J0538+2817 in S147”. *ApJ*, 654, 487
- Papageorgiou, A., Cawthorne, T. V., Stirling, A., et al. 2006, “Space very long baseline interferometry observations of polarization in the jet of 3C380”. *MNRAS*, 373, 449
- Pauliny-Toth, I. I. K. and Kellermann, K. I. 1966, “Variations in the Flux Densities of Radio Sources.” *AJ*, 71, 394
- Pearson, T. J. and Readhead, A. C. S. 1988, “The milliarcsecond structure of a complete sample of radio sources. II - First-epoch maps at 5 GHz”. *ApJ*, 328, 114
- Peck, A. B., Henkel, C., Ulvestad, J. S., et al. 2003, “The Flaring H₂O Megamaser and Compact Radio Source in Markarian 348”. *ApJ*, 590, 149
- Peck, A. B. and Taylor, G. B. 2001, “Evidence for a Circumnuclear Disk in 1946+708”. *ApJ*, 554, L147
- Peck, A. B., Taylor, G. B., and Conway, J. E. 1999, “Obscuration of the Parsec-Scale Jets in the Compact Symmetric Object 1946+708”. *ApJ*, 521, 103
- Perucho, M. and Lobanov, A. P. 2007, “Physical properties of the jet in 0836+710 revealed by its transversal structure”. *A&A*, 469, L23
- Perucho, M., Lobanov, A. P., Martí, J.-M., et al. 2006, “The role of Kelvin-Helmholtz instability in the internal structure of relativistic outflows. The case of the jet in 3C 273”. *A&A*, 456, 493
- Piner, B. G., Bhattarai, D., Edwards, P. G., et al. 2006, “The Fastest Relativistic Jets: VLBA Observations of Blazars with Apparent Speeds Exceeding 25c”. *ApJ*, 640, 196
- Pollack, L. K., Taylor, G. B., and Zavala, R. T. 2003, “VLBI Polarimetry of 177 Sources from the Caltech-Jodrell Bank Flat-Spectrum Survey”. *ApJ*, 589, 733
- Porcas, R. W., “VLBI Observations of gravitational lenses”, in: F. Mantovani and A. Kus (eds.), *The Role of VLBI in Astrophysics, Astrometry and Geodesy. Proceedings of the NATO Advanced Study Institute, held September 17-29, 2001, in Bologna, Italy. Series II, mathematics, physics and chemistry, Vol. 135.* Edited by Franco Mantovani and Andrzej Kus. ISBN 1-4020-1875-4: ISBN 1-4020-2406-1 (e-book). Published by Kluwer Academic Publishers, Dordrecht, The Netherlands, 2004, p.219, p. 219 (2004)

- Porcas, R. W., Garrett, M. A., and Nair, S., “EVN–MERLIN/Global observations of the Gravitational Lens MG 2016+112”, in: E. Ros, R. W. Porcas, A. P. Lobanov, and J. A. Zensus (eds.), *Proceedings of the 6th EVN Symposium*, p. 197 (2002)
- Pradel, N., Charlot, P., and Lestrade, J.-F. 2006, “Astrometric accuracy of phase-referenced observations with the VLBA and EVN”. *A&A*, 452, 1099
- Pushkarev, A. B., Gabuzda, D. C., Vetukhnovskaya, Y. N., et al. 2005, “Spine-sheath polarization structures in four active galactic nuclei jets”. *MNRAS*, 356, 859
- Pyatunina, T. B., Kudryavtseva, N. A., Gabuzda, D. C., et al. 2006, “Frequency-dependent time-delays for strong outbursts in selected blazars from the Metsähovi and the University of Michigan Radio Astronomy Observatory monitoring databases - I.” *MNRAS*, 373, 1470
- Qian, S., Kraus, A., Zhang, X., et al. 2002, “Multifrequency Polarization Variations in the Quasar 0917+624”. *Chinese Journal of Astronomy and Astrophysics*, 2, 325
- Qian, S., Li, X., Wegner, R., et al. 1996, “Implications of the correlation between the optical and radio intraday variations in BLO 0716+714”. *Chinese Astronomy and Astrophysics*, 20, 15
- Qian, S. and Zhang, X. 2004, “An Intrinsic Model for the Polarization Position Angle Swing Observed in QSO 1150+812”. *Chinese Journal of Astronomy and Astrophysics*, 4, 37
- Qian, S. J., Quirrenbach, A., Witzel, A., et al. 1991, “A model for the rapid radio variability in the quasar 0917 + 624”. *A&A*, 241, 15
- Quataert, E. and Gruzinov, A. 2000, “Convection-dominated Accretion Flows”. *ApJ*, 539, 809
- Quirrenbach, A., Witzel, A., Kirchbaum, T. P., et al. 1992, “Statistics of intraday variability in extragalactic radio sources”. *A&A*, 258, 279
- Quirrenbach, A., Witzel, A., Qian, S. J., et al. 1989, “Rapid radio polarization variability in the quasar 0917 + 624”. *A&A*, 226, L1
- Quirrenbach, A., Witzel, A., Wagner, S., et al. 1991, “Correlated radio and optical variability in the BL Lacertae object 0716 + 714”. *ApJ*, 372, L71
- Readhead, A. C. S. 1994, “Equipartition brightness temperature and the inverse Compton catastrophe”. *ApJ*, 426, 51
- Readhead, A. C. S., Taylor, G. B., Pearson, T. J., et al. 1996, “Compact Symmetric Objects and the Evolution of Powerful Extragalactic Radio Sources”. *ApJ*, 460, 634

- Rees, M. J. 1967, “Studies in radio source structure-I. A relativistically expanding model for variable quasi-stellar radio sources”. *MNRAS*, 135, 345
- Refsdal, S. 1964, “On the possibility of determining Hubble’s parameter and the masses of galaxies from the gravitational lens effect”. *MNRAS*, 128, 307
- Reid, M. J., Biretta, J. A., Junor, W., et al. 1989, “Subluminal motion and limb brightening in the nuclear jet of M87”. *ApJ*, 336, 112
- Reid, M. J., Readhead, A. C. S., Vermeulen, R. C., et al. 1999, “The Proper Motion of Sagittarius A*. I. First VLBA Results”. *ApJ*, 524, 816
- Rickett, B. J. 2001, “Radio Sources and Scintillation”. *Ap&SS*, 278, 5
- Rickett, B. J., Quirrenbach, A., Wegner, R., et al. 1995, “Interstellar scintillation of the radio source 0917+624.” *A&A*, 293, 479
- Rickett, B. J., Witzel, A., Kraus, A., et al. 2001, “Annual Modulation in the Intraday Variability of Quasar 0917+624 due to Interstellar Scintillation”. *ApJ*, 550, L11
- Rogers, A. E. E., Doeleman, S., Wright, M. C. H., et al. 1994, “Small-scale structure and position of Sagittarius A* from VLBI at 3 millimeter wavelength”. *ApJ*, 434, L59
- Rohlfs, K., Tools of radio astronomy (Berlin and New York, Springer-Verlag, 1986, 332 p., 1986)
- Romney, J. D., “Cross Correlators”, in: G. B. Taylor, C. L. Carilli, and R. A. Perley (eds.), *Synthesis Imaging in Radio Astronomy II*, vol. 180 of *Astronomical Society of the Pacific Conference Series*, p. 57 (1999)
- Rowan-Robinson, M. 1977, “On the unity of activity in galaxies”. *ApJ*, 213, 635
- Rupen, M. P., “Spectral Line Observing II: Calibration and Analysis”, in: G. B. Taylor, C. L. Carilli, and R. A. Perley (eds.), *Synthesis Imaging in Radio Astronomy II*, vol. 180 of *Astronomical Society of the Pacific Conference Series*, p. 229 (1999)
- Rusin, D., Norbury, M., Biggs, A. D., et al. 2002, “High-resolution observations and mass modelling of the CLASS gravitational lens B1152+199”. *MNRAS*, 330, 205
- Ryle, M. and Hewish, A. 1960, “The synthesis of large radio telescopes”. *MNRAS*, 120, 220
- Sandstrom, K. M., Peek, J. E. G., Bower, G. C., et al. 2007, “A Parallax Distance of $389 \pm 24/-21$ parsecs to the Orion Nebula Cluster from Very Long Baseline Array Observations”. *ArXiv e-prints*, 706

- Savolainen, T., Wiik, K., Valtaoja, E., et al. 2002, “Connections between millimetre continuum variations and VLBI structure in 27 AGN”. *A&A*, 394, 851
- Schechter, P. L. 2005, “The Hubble Constant from Gravitational Lens Time Delays”. 225, 281
- Scheuer, P. A. G. and Readhead, A. C. S. 1979, “Superluminally expanding radio sources and the radio-quiet QSOs”. *Nature*, 277, 182
- Shen, Z.-Q., Lo, K. Y., Liang, M.-C., et al. 2005, “A size of ~ 1 AU for the radio source Sgr A* at the centre of the Milky Way”. *Nature*, 438, 62
- Sholomitskii, G. B. 1965, “Fluctuations in the 32.5-cm Flux of CTA 102”. *Soviet Astronomy*, 9, 516
- Sikora, M., Begelman, M. C., Madejski, G. M., et al. 2005, “Are Quasar Jets Dominated by Poynting Flux?” *ApJ*, 625, 72
- Stappers, B. W., Gaensler, B. M., and Johnston, S. 1999, “A deep search for pulsar wind nebulae using pulsar gating”. *MNRAS*, 308, 609
- Stirling, A. M., Cawthorne, T. V., Stevens, J. A., et al. 2003, “Discovery of a precessing jet nozzle in BL Lacertae”. *MNRAS*, 341, 405
- Szomoru, A., Biggs, A., Garrett, M., et al., “From truck to optical fibre: the coming-of-age of eVLBI”, in: R. Bachiller, F. Colomer, J.-F. Desmurs, and P. de Vicente (eds.), *European VLBI Network on New Developments in VLBI Science and Technology*, pp. 257–260 (2004)
- Taylor, G. B., Carilli, C. L., Perley, R. A., et al. (eds.), *Synthesis Imaging in Radio Astronomy II* (1999)
- Taylor, G. B., Vermeulen, R. C., Readhead, A. C. S., et al. 1996, “A Complete Flux-Density-limited VLBI Survey of 293 Flat-Spectrum Radio Sources”. *ApJS*, 107, 37
- Thompson, A. R., Moran, J. M., and Swenson, G. W., *Interferometry and synthesis in radio astronomy* (New York, Wiley-Interscience, 692 p., 2nd ed., 2001)
- Tingay, S. J., Preston, R. A., Lister, M. L., et al. 2001, “Measuring the Brightness Temperature Distribution of Extragalactic Radio Sources with Space VLBI”. *ApJ*, 549, L55
- Torres, R. M., Loinard, L., Mioduszewski, A. J., et al. 2007, “VLBA determination of the distance to nearby star-forming regions II. Hubble 4 and HDE 283572 in Taurus”. *ArXiv e-prints*, 708

- Ulvestad, J. S., “VLBI Imaging of Seyfert Galaxies”, in: J. A. Zensus, M. H. Cohen, and E. Ros (eds.), *Radio Astronomy at the Fringe*, vol. 300 of *Astronomical Society of the Pacific Conference Series*, p. 97 (2003)
- Ulvestad, J. S., Antonucci, R. R. J., and Barvainis, R. 2005, “VLBA Imaging of Central Engines in Radio-Quiet Quasars”. *ApJ*, 621, 123
- Ulvestad, J. S., Johnson, K. E., and Neff, S. G. 2007, “A VLBI Search for Radio Supernovae in Wolf-Rayet Galaxies”. *AJ*, 133, 1868
- Urry, C. M. and Padovani, P. 1995, “Unified Schemes for Radio-Loud Active Galactic Nuclei”. *PASP*, 107, 803
- van Langevelde, H. J., Pihlström, Y. M., Conway, J. E., et al. 2000, “A thin H I circumnuclear disk in NGC 4261”. *A&A*, 354, L45
- Vermeulen, R. C., Pihlström, Y. M., Tschager, W., et al. 2003, “Observations of H I absorbing gas in compact radio sources at cosmological redshifts”. *A&A*, 404, 861
- Vlahakis, N. and Königl, A. 2004, “Magnetic Driving of Relativistic Outflows in Active Galactic Nuclei. I. Interpretation of Parsec-Scale Accelerations”. *ApJ*, 605, 656
- Vlemmings, W. H. T., Diamond, P. J., and Imai, H. 2006a, “A magnetically collimated jet from an evolved star”. *Nature*, 440, 58
- Vlemmings, W. H. T., Diamond, P. J., and van Langevelde, H. J. 2002, “Circular polarization of water masers in the circumstellar envelopes of late type stars”. *A&A*, 394, 589
- Vlemmings, W. H. T., Diamond, P. J., van Langevelde, H. J., et al. 2006b, “The magnetic field in the star-forming region Cepheus A from H₂O maser polarization observations”. *A&A*, 448, 597
- Vlemmings, W. H. T. and van Langevelde, H. J. 2007, “Improved VLBI astrometry of OH maser stars”. *A&A*, 472, 547
- Vlemmings, W. H. T., van Langevelde, H. J., and Diamond, P. J. 2005, “The magnetic field around late-type stars revealed by the circumstellar H₂O masers”. *A&A*, 434, 1029
- Wagner, S., Sanchez-Pons, F., Quirrenbach, A., et al. 1990, “Simultaneous optical and radio monitoring of rapid variability in quasars and BL Lac objects”. *A&A*, 235, L1
- Wagner, S. J., Witzel, A., Heidt, J., et al. 1996, “Rapid Variability in S5 0716+714 Across the Electromagnetic Spectrum”. *AJ*, 111, 2187

- Walker, R. C., “Very Long Baseline Interferometry”, in: G. B. Taylor, C. L. Carilli, and R. A. Perley (eds.), *Synthesis Imaging in Radio Astronomy II*, vol. 180 of *Astronomical Society of the Pacific Conference Series*, pp. 433–462 (1999)
- Walker, R. C., Dhawan, V., Romney, J. D., et al. 2000, “VLBA Absorption Imaging of Ionized Gas Associated with the Accretion Disk in NGC 1275”. *ApJ*, 530, 233
- Wardle, J. F. C. and Homan, D. C. 2003, “Theoretical Models for Producing Circularly Polarized Radiation in Extragalactic Radio Sources”. *Ap&SS*, 288, 143
- Wardle, J. F. C., Homan, D. C., Ojha, R., et al. 1998, “Electron-positron jets associated with the quasar 3C279”. *Nature*, 395, 457
- Weiler, K. W. and de Pater, I. 1983, “A catalog of high accuracy circular polarization measurements”. *ApJS*, 52, 293
- Westpfahl, D. J., “Spectral-Line Observing I: Introduction”, in: G. B. Taylor, C. L. Carilli, and R. A. Perley (eds.), *Synthesis Imaging in Radio Astronomy II*, vol. 180 of *Astronomical Society of the Pacific Conference Series*, p. 201 (1999)
- Whitney, A. R., Shapiro, I. I., Rogers, A. E. E., et al. 1971, “Quasars Revisited: Rapid Time Variations Observed Via Very-Long-Baseline Interferometry”. *Science*, 173, 225
- Wilson, A. S. and Colbert, E. J. M. 1995, “The difference between radio-loud and radio-quiet active galaxies”. *ApJ*, 438, 62
- Witzel, A., Heeschen, D. S., Schalinski, C., et al. 1986, “Kurzzeit-Variabilität extragalaktischer Radioquellen”. *Mitteilungen der Astronomischen Gesellschaft Hamburg*, 65, 239
- Yi, J., Booth, R. S., Conway, J. E., et al. 2005, “SiO masers in TX Cam. Simultaneous VLBA observations of two 43 GHz masers at four epochs”. *A&A*, 432, 531
- York, T., Jackson, N., Browne, I. W. A., et al. 2005, “The Hubble constant from the gravitational lens CLASS B0218+357 using the Advanced Camera for Surveys”. *MNRAS*, 357, 124
- Yuan, F., Markoff, S., and Falcke, H. 2002, “A Jet-ADAF model for Sgr A*”. *A&A*, 383, 854
- Zavala, R. T. and Taylor, G. B. 2003, “A View through Faraday’s Fog: Parsec-Scale Rotation Measures in Active Galactic Nuclei”. *ApJ*, 589, 126
- Zavala, R. T. and Taylor, G. B. 2004, “A View through Faraday’s Fog. II. Parsec-Scale Rotation Measures in 40 Active Galactic Nuclei”. *ApJ*, 612, 749

- Zensus, J. A., Ros, E., Kellermann, K. I., et al. 2002, “Sub-milliarcsecond Imaging of Quasars and Active Galactic Nuclei. II. Additional Sources”. *AJ*, 124, 662
- Zhang, J. S., Henkel, C., Kadler, M., et al. 2006, “Extragalactic H₂O masers and X-ray absorbing column densities”. *A&A*, 450, 933